Structure, Bonding, and Dynamic Behavior of Bis(η^2-ethylene)hexakis(neopentoxy)ditungsten. Studies of the Reversible Addition of C–C Double Bonds to a W–W Triple Bond[1]

Stephanie T. Chacon, Malcolm H. Chisholm,* Odile Eisenstein, and John C. Huffman

Contribution from the Department of Chemistry and Molecular Structure Center, Indiana University, Bloomington, Indiana 47405, and Laboratoire de Chimie Théorique, Bâtiment 490, Centre de Paris-Sud, 91405 Orsay, France. *Received April 20, 1992*

Abstract: Hydrocarbon solutions of $W_2(OCH_2\text{-}t\text{-}Bu)_6$ and ethylene (≥2 equiv) react at 0 °C to yield $W_2(OCH_2\text{-}t\text{-}Bu)_6(\eta^2\text{-}C_2H_4)_2$, **1**, which has been characterized by NMR studies and a single-crystal X-ray diffraction study. Crystal data for **1** at −155 °C: a = 11.754 (4) Å, b = 31.405 (14) Å, c = 11.274 (4) Å, β = 104.96 (2)°, Z = 4, d_{calcd} = 1.564 g cm^{-3}, and space group $P2_1/c$. The molecular structure of **1** has virtual C_2 symmetry. There are four bridging OR ligands that span a W–W bond of distance 2.533 (1) Å in an unsymmetrical manner; W–O (bridge) = 2.00 (1) and 2.31 (1) Å (av) for the four short and four long distances, respectively. The long W–O distances are trans to terminal W–OR or W–(η^2-C_2H_4) ligands. The dinuclear molecule may be viewed as a dimer of two pseudotetrahedral $W(OR)_3(\eta^2\text{-}C_2H_4)$ moieties and the $W(\eta^2\text{-}C_2H_4)$ fragments are metallacyclopropanes: C–C = 1.45 (2) Å and W–C = 2.14 (2) Å (av). The alignment of the two olefinic C_2 axes are mutually orthogonal and perpendicular to the W–W axis. This arises from the mutual competition of W d_π–olefin π^* bonding and W–W bonding. In solution, compound **1** is in equilibrium with $W_2(OCH_2\text{-}t\text{-}Bu)_6$ and C_2H_4 and above 0 °C reacts further with ethylene to yield $W_2(OCH_2\text{-}t\text{-}Bu)_6(\mu\text{-}CCH_2CH_2CH_2)$ and ethane by way of an intermediate metallacyclopentane–ethylene complex $W_2(OCH_2\text{-}t\text{-}Bu)_6(CH_2)_4(\eta^2\text{-}C_2H_4)$ [*J. Am. Chem. Soc.* **1989**, *111*, 5284]. At −20 °C the ^{1}H and ^{13}C{^{1}H} NMR spectra are consistent with those expected on the basis of the solid-state structure. By a combination of C–H/C–D labeling and nuclear Overhauser enhancement (NOE) difference spectroscopy, an assignment of the four ethylenic and six methylenic protons (of the OR ligands) has been made. Spin saturation transfer difference spectroscopic studies of **1** in toluene-d_8 in the temperature range 5–25 °C reveal a dynamic process that is distinct from the equilibrium involving **1** and $W_2(OCH_2\text{-}t\text{-}Bu)_6$ and C_2H_4. The selective site exchange amongst the C–H protons is consistent with the pairwise opening and closing of OR bridges about an intermediate that has C_{2v} symmetry $(W_2(\mu\text{-}OR)_2(OR)_4(\eta^2\text{-}C_2H_4)_2)$ and is related to the previously characterized compound $W_2(CH_2Ph)_2(\mu\text{-}O\text{-}i\text{-}Pr)_2(O\text{-}i\text{-}Pr)_2(\eta^2\text{-}C_2Me_2)_2$. The activation parameters for the fluxional behavior of **1** are $\Delta H^* = 13.4 \pm 0.9$ kcal mol^{-1} and $\Delta S^* = -13 \pm 3$ cal K^{-1} mol^{-1}. The bonding in **1** was investigated by MO calculations on the hypothetical molecule $W_2(OH)_6(\eta^2\text{-}C_2H_4)_2$ with structural data taken from the X-ray study of **1**. The calculations employed the method of Fenske and Hall and extended Hückel theory. Calculations were also carried out on the doubly bridged species $W_2(\mu\text{-}OH)_2(OH)_4(\eta^2\text{-}C_2H_4)_2$, which has a structure based on the fusing of two square-based pyramids. In these geometries, rotation about the W–C_2 olefin axis is not restricted in the manner seen in the ground-state geometry. Attempts to determine the role of **1** in the formation of the metallacyclopentane–ethylene complex $W_2(OCH_2\text{-}t\text{-}Bu)_6(CH_2)_4(\eta^2\text{-}C_2H_4)$ were partially obscured by the competitive reversible formation of **1** from $W_2(OCH_2\text{-}t\text{-}Bu)_6$ and ethylene. In the presence of a large excess of ethylene (10, 20, and 30 equiv), the disappearance of **1** and conversion to $W_2(OCH_2\text{-}t\text{-}Bu)_6(CH_2)_4(\eta^2\text{-}C_2H_4)$ and $W_2(OCH_2\text{-}t\text{-}Bu)_6(\mu\text{-}CCH_2CH_2CH_2)$ is independent of the concentration of C_2H_4 and first order in **1**.

Introduction

Small clusters of molybdenum and tungsten supported by alkoxide ligands provide templates for organometallic chemistry by substrate uptake and activation.[2] The presence of more than one metal atom facilitates multisite activation which may lead to coupling of ligands or their degradation depending upon the conditions. Examples have been noted wherein extremely strong bonds have been cleaved, as in the previous report of the conversion of carbon monoxide to carbido (C^{4-}) and oxo (O^{2-}) ligands,[3] or coupled, as in the sequence involving alkyne oligomerization.[4] Novel modes of ligand binding have also been seen, e.g., in the allene adduct $W_2(O\text{-}t\text{-}Bu)_6(\mu\text{-}CH_2CCH_2)$[5] and the butadiene adduct $W_2(OCH_2\text{-}t\text{-}Bu)_6(C_4H_6)(py)$.[6] The M–M bonding electrons provide an electron reservoir for substrate uptake and release, and the alkoxide ligands act as versatile spectator groups, being capable of variable electron donation ($\sigma^2 + \pi^x$) and being readily interconverted between terminal and bridging modes. The steric pressure exerted at the metal center can be modified as a function of the alkyl group R to make a given $M_n(OR)_x$ complex substrate selective.

Previously we reported on the reactions between $W_2(OR)_6$ compounds (see structure A below) and ethylene which proceed according to the overall stoichiometry shown in eq 1.[7]

$$W_2(OR)_6 + 3C_2H_4 \rightarrow W_2(OR)_6(\mu\text{-}CCH_2CH_2CH_2) + C_2H_6 \quad (1)$$

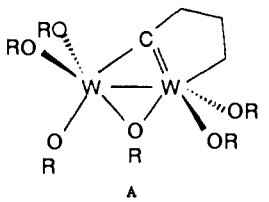

A

(1) Metal Alkoxides. Models for Metal Oxides. 18. For the previous paper in this series, see: Chisholm, M. H.; Hammond, C. E.; Johnston, V. J.; Streib, W. E.; Huffman, J. C. *J. Am. Chem. Soc.* **1992**, *114*, 7056.

(2) Chisholm, M. H.; Clark, D. L.; Hampden-Smith, M. J.; Hoffman, D. M. *Angew. Chem., Int. Ed. Engl.* **1989**, *28*, 432.

(3) (a) Chisholm, M. H.; Folting, K.; Hampden-Smith, M. J.; Hammond, C. E. *J. Am. Chem. Soc.* **1989**, *111*, 7283. (b) Chisholm, M. H.; Hammond, C. E.; Huffman, J. C.; Johnston, V. J. *J. Organomet. Chem.* **1990**, *394*, C16. (c) Reference 1.

(4) Chisholm, M. H.; Hoffman, D. M.; Huffman, J. C. *J. Am. Chem. Soc.* **1984**, *106*, 6806.

(5) (a) Cayton, R. H.; Chacon, S. T.; Chisholm, M. H.; Hampden-Smith, M. J.; Huffman, J. C.; Folting, K.; Ellis, P.; Huggins, B. A. *Angew. Chem., Int. Ed. Engl.* **1989**, *28*, 1523. (b) Chacon, S. T.; Chisholm, M. H.; Folting, K.; Huffman, J. C.; Hampden-Smith, M. J. *Organometallics* **1991**, *10*, 3722.

(6) Chisholm, M. H.; Huffman, J. C.; Lucas, E. A.; Lobkovsky, E. B. *Organometallics* **1991**, *10*, 3424.

(7) Chisholm, M. H.; Huffman, J. C.; Hampden-Smith, M. J. *J. Am. Chem. Soc.* **1989**, *111*, 5284.

0002-7863/92/1514-8497$03.00/0

Scheme I

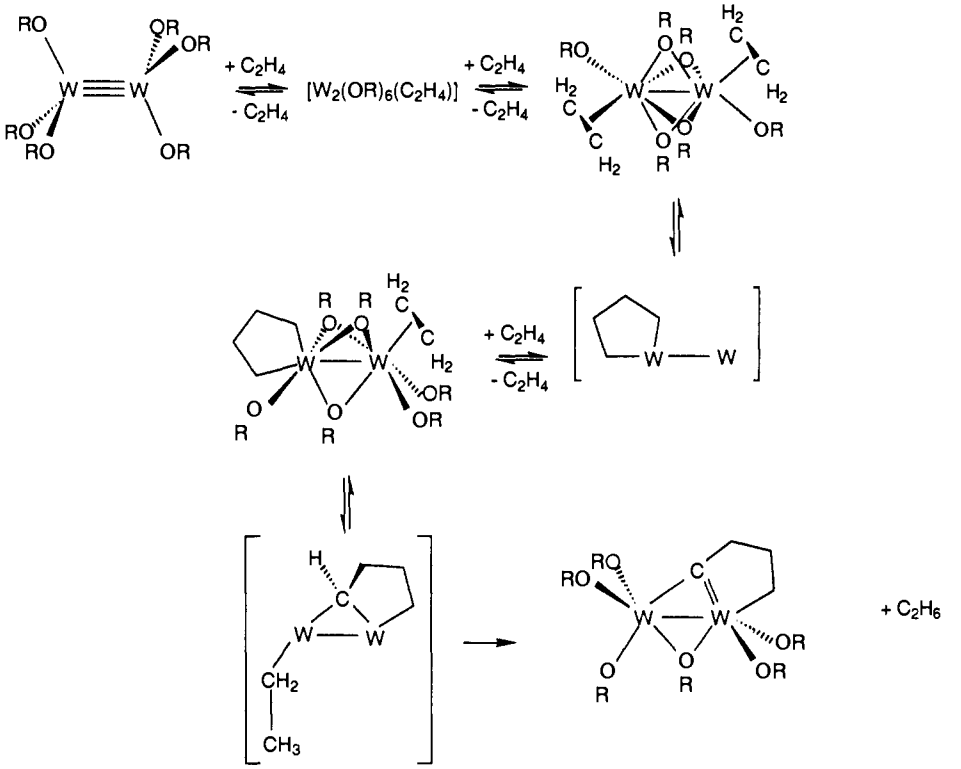

The relative rates of reaction **1** were qualitatively shown to follow the order R = *i*-Pr > c-Pen > c-Hex > CH_2-*t*-Bu ≫ *t*-Bu (for which no reaction was observed at room temperature).

In the case of R = *i*-Pr, a metallacyclopentane–ethylene complex, $W_2(O\text{-}i\text{-}Pr)_6(CH_2)_4(\eta^2\text{-}C_2H_4)$ was formed *reversibly* (eq 2) and was structurally characterized. (See B below.)

$$W_2(O\text{-}i\text{-}Pr)_6 + 3C_2H_4 \rightleftarrows W_2(O\text{-}i\text{-}Pr)_6(CH_2)_4(\eta^2\text{-}C_2H_4) \quad (2)$$

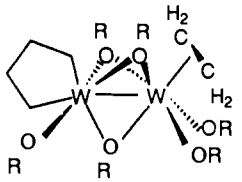

B

The role of the metallacyclopentane–ethylene complex in the formation of the alkylidyne-bridged metallacycle (eq 1) was investigated by the use of labeled ethylene. The initial reversible formation of $W_2(O\text{-}i\text{-}Pr)_6(CH_2)_4(\eta^2\text{-}C_2H_4)$ occurs without C–H activation and without C_2 bond cleavage. Further studies of the reaction shown in eq 3 reveal that, although exchange between

$W_2(O\text{-}i\text{-}Pr)_6(CH_2)_4(\eta^2\text{-}C_2H_4) + n^*C_2H_4 \rightarrow$

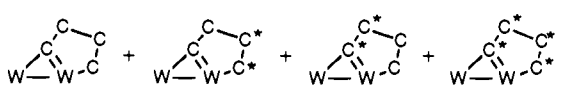

(3)

coordinated and free ethylene occurs with ease, the greater the excess of added ethylene ($^*C_2H_4$) the less $^*C_2$ is incorporated within the μ-alkylidyne ligand.

Incorporation of $^*C_2$ units into the alkylidyne bridge compounds occurs in a pairwise manner, again consistent with retention of the original C–C bond of each C_2H_4 unit. These observations lead us to propose the general reaction sequence shown in Scheme I. Although no mono-ethylene complex has been detected, a bis-ethylene complex has been isolated for R = CH_2-*t*-Bu. We report here our characterization of this complex. This work provides the first example of the cooperative binding of two independent C–C double bonds to a W–W triple bond. We also report further studies of the reactivity of this complex. A preliminary account has appeared.[8]

Results and Discussion

Synthesis of $W_2(OCH_2\text{-}t\text{-}Bu)_6(\eta^2\text{-}C_2H_4)_2$. Hydrocarbon solutions of $W_2(OCH_2\text{-}t\text{-}Bu)_6$ and ethylene react reversibly at room temperature to give $W_2(OCH_2\text{-}t\text{-}Bu)_6(\eta^2\text{-}C_2H_4)_2$ (**1**) according to eq 4.

$$W_2(OCH_2\text{-}t\text{-}Bu)_6 + 2C_2H_4 \rightleftarrows \underset{\mathbf{1}}{W_2(OCH_2\text{-}t\text{-}Bu)_6(\eta^2\text{-}C_2H_4)_2} \quad (4)$$

We have not seen any evidence by NMR spectroscopy for a mono-ethylene intermediate, and as such the mono-ethylene complex must be labile with respect to uptake of ethylene and ethylene dissociation. The overall reaction between $W_2(OCH_2\text{-}t\text{-}Bu)_6$ and ethylene proceeds as shown in eq 1 to give the alkylidyne-bridged metallacyclic compound, and the intermediacy of the metallacyclopentane–ethylene complex $W_2(OCH_2\text{-}t\text{-}Bu)_6(CH_2)_4(\eta^2\text{-}C_2H_4)$ can be seen from NMR studies. This reactivity (eq 1) has prevented us from examining the equilibrium 4 and the determination of thermodynamic and activation parameters. At −20 °C equilibrium 4 lies extensively in favor of **1** and the conversion to the alkylidyne complex (eq 1) is slow, $t_{1/2}$ ≈ several days. At −40 °C reaction 1 requires several weeks. Studies of equilibrium 4 involving the labeled ethylenes *cis*-, *trans*-, and *gem*-$C_2H_2D_2$ did not reveal any isomerization of the ethylenes.[8b] When ca. 10 mg of **1** is dissolved in 0.3 mL of toluene-d_8 at −72 °C and the NMR tube is sealed with a torch, ethylene dissociation occurs upon warming to 22 °C to give roughly equal quantities of **1** and $W_2(OCH_2\text{-}t\text{-}Bu)_6$. Compound **1** is favored in the presence of an excess (≥10 equiv) of ethylene under these conditions. While this parallels many other Lewis base reactions (eq 5), equilibrium 4 is notably slower. Specifically, while eq 5 for L = py, $HNMe_2$, or PMe_3 is fast on the ^1H NMR timescale,[9] equilibrium 4, though chemically rapid, is not rapid enough to cause line broadening in the NMR spectrum.

(8) (a) Cayton, R. H.; Chacon, S. T.; Chisholm, M. H.; Huffman, J. C. *Angew. Chem., Int. Ed. Engl.* **1990**, *29*, 1026. (b) Chisholm, M. H.; Hampden-Smith, M. J. *Angew. Chem., Int. Ed. Engl.* **1987**, *26*, 903.

$$W_2(OR)_6 + 2L \rightleftarrows W_2(OR)_6L_2 \quad (5)$$

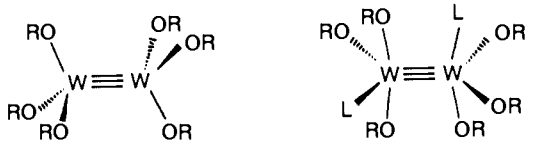

Presumably the greater kinetic barrier to the formation of **1** in eq 4 reflects the greater requirements in the reorganization of the metal center, namely, the rehybridization required for olefin coordination.

The optimum preparation of **1** involved the addition of 2 equiv of C_2H_4 to a cooled solution of $W_2(OCH_2\text{-}t\text{-}Bu)_6$ in hexane (−10 °C, 2 h) followed by crystallization at −20 °C. Compound **1** is an air-stable (for periods of hours), yellow crystalline solid. Compound **1** slowly decomposes in the solid state at 22 °C under an inert atmosphere but may be stored at −20 °C for several months.

The highest molecular weight ion detected in the mass spectrum corresponded to $W_2(OCH_2\text{-}t\text{-}Bu)_6^+$, which indicates loss of the two ethylene ligands.

Since $W_2(OCH_2\text{-}t\text{-}Bu)_6$ is prepared from the reaction between $W_2(O\text{-}t\text{-}Bu)_6$ and neopentanol (≥6 equiv) and $W_2(OCH_2\text{-}t\text{-}Bu)_6$ is coordinatively unsaturated, it is important that the $W_2(OCH_2\text{-}t\text{-}Bu)_6$ starting material is completely free of coordinated alcohol. This is because there is an additional reaction involving $W_2(OCH_2\text{-}t\text{-}Bu)_6$ and ethylene in the presence of ROH as shown in eq 6.[10] Though eq 6 is slow at low temperature (below 0 °C),

$$W_2(OCH_2\text{-}t\text{-}Bu)_6 + 2C_2H_4 + ROH \xrightarrow[4\ days]{22\ °C} W_2(OCH_2\text{-}t\text{-}Bu)_6(OR)(\mu\text{-}CCH_3) + C_2H_6 \quad (6)$$

$$R = t\text{-}Bu \text{ or } CH_2\text{-}t\text{-}Bu$$

it still may compete with the efficient preparation of **1**.

Solid-State and Molecular Structure. In the space group $P2_1/c$, there are four molecules in the unit cell, and these exist as two pairs of enantiomers. The molecular structure of one enantiomer is shown in Figures 1 and 2. The view in Figure 1 reveals most clearly the presence of the four bridging $OCH_2\text{-}t\text{-}Bu$ ligands and that there are only two terminal ligands per tungsten atom, namely, one alkoxide and one ethylene. This is the first such example for the chemistry of W_2^{6+}-containing compounds. The view in Figure 2 more clearly shows the presence of the virtual C_2 axis and also emphasizes the orthogonality of the ethylenic C_2 axes which are perpendicular to the W–W axis. One can also see how in this structure the W–O bonds lie within two mutually perpendicular planes.

Fractional coordinates are given in Table I, and selected bond distances and angles are given in Tables II and III, respectively. A summary of crystal data is given in Table IV.

The olefinic C–C distances, 1.45 (2) Å (av), are notably longer than that in free ethylene, 1.339 Å,[11] which, when taken together with the relatively short W–C distances, 2.14 (2) Å (av), leads us to suggest that the WC_2 fragments may be viewed as approaching the limiting valence bond description of a metallacyclopropane. For comparison we list some structural and NMR parameters for other early transition metal–ethylene complexes in Table V.

The W–W distance of 2.533 (1) Å is notably longer than the W≡W bond distances in $W_2(OR)_6$ compounds, which fall in the range of 2.3–2.4 Å,[12] and falls in the range typically ascribed to W–W double bonds in dinuclear compounds.[9] However, the presence of four bridging ligands is unique, and it is worth noting

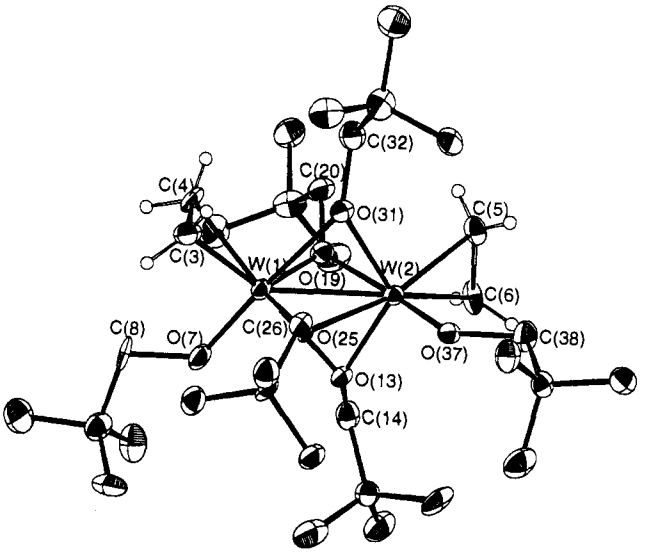

Figure 1. ORTEP diagram of $W_2(OCH_2\text{-}t\text{-}Bu)_6(\eta^2\text{-}C_2H_4)_2$ (**1**), looking perpendicular to the W–W bond axis with 50% thermal ellipsoids showing numbering scheme for the atoms. Alkoxide protons have been removed for clarity.

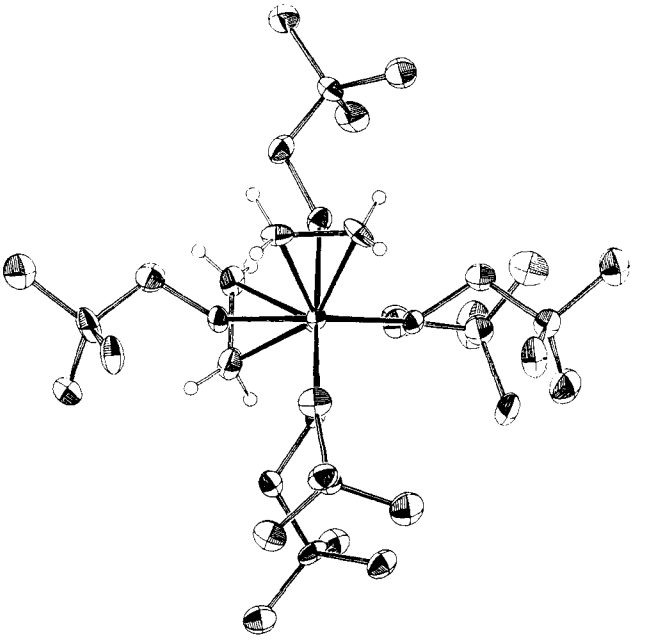

Figure 2. ORTEP diagram of $W_2(OCH_2\text{-}t\text{-}Bu)_6(\eta^2\text{-}C_2H_4)_2$ (**1**), looking down the W–W bond axis with 50% thermal ellipsoids. Alkoxide protons have been removed for clarity.

that in triangular clusters such as $W_3(\mu_3\text{-}O)(\mu_3\text{-}OR)(\mu\text{-}OR)_3(OR)_6$ the W–W distances are 2.54 Å and are assigned as W–W single bonds.[13] Suffice it to say that an assignment of M–M bond order on the basis of M–M distance alone, particularly in the presence of bridging ligands, is not reliable but is merely an indicator of the possibilities. However, in terms of a limiting assignment, if the coordinated ethylene is considered as a $C_2H_4^{2-}$ ligand, i.e., a metallacyclopropane, then the formal oxidation state of the tungsten atoms is 5+, providing therefore a W_2^{10+} core with a W–W single bond.

Another notable feature of the structure is the presence of the asymmetric alkoxide bridges. Each bridge has a short (ca. 2.00 (1) Å (av) and a long (2.31 (1) Å (av)) W–O bond distance. The long bonds are trans to the terminal C_2H_4 and $OCH_2\text{-}t\text{-}Bu$ ligands. Also, the atoms W_2OC associated with the bridging alkoxide

(9) Chisholm, M. H. *Polyhedron* **1983**, *2*, 681.
(10) Chacon, S. T.; Chisholm, M. H.; Cook, C. M.; Hampden-Smith, M. J.; Streib, W. E. *Angew. Chem., Int. Ed. Engl.* **1992**, *31*, 462.
(11) Stoicheff, B. P. *Tetrahedron* **1962**, *17*, 135.
(12) (a) R = i-Pr: Chisholm, M. H.; Clark, D. L.; Folting, K.; Huffman, J. C.; Hampden-Smith, M. J. *J. Am. Chem. Soc.* **1987**, *109*, 7750. (b) R = c-hexyl and $(RO)_2$ = $Me_2C(O)C(O)Me_2$: Chisholm, M. H.; Folting, K.; Hampden-Smith, M. J.; Smith, C. A. *Polyhedron* **1987**, *6*, 1747.
(13) Chisholm, M. H.; Folting, K.; Huffman, J. C.; Kober, E. M. *Inorg. Chem.* **1985**, *24*, 241.

Table I. Fractional Coordinates and Isotropic Thermal Parameters for $W_2(OCH_2$-t-$Bu)_6(\eta^2$-$C_2H_4)_2$ (1)

atom	10^4x	10^4y	10^4z	$10B_{iso}$	atom	10^4x	10^4y	10^4z	$10B_{iso}$
W(1)	7741.5 (4)	940.2 (1)	4274.2 (4)	12	C(22)	10280 (11)	724 (4)	2730 (12)	24
W(2)	6309.4 (4)	1439.2 (1)	2870.9 (4)	13	C(23)	9498 (12)	526 (4)	515 (12)	29
C(3)	7437 (10)	344 (4)	5032 (11)	19	C(24)	9627 (11)	1291 (4)	1146 (12)	26
C(4)	8092 (10)	278 (4)	4119 (11)	19	O(25)	6477 (6)	1222 (2)	4873 (6)	13
C(5)	5756 (10)	1475 (4)	904 (10)	19	C(26)	5588 (10)	1074 (4)	5421 (11)	19
C(6)	6561 (10)	1821 (4)	1374 (11)	22	C(27)	5774 (10)	1238 (4)	6707 (10)	19
O(7)	9199 (6)	1065 (2)	5400 (6)	14	C(28)	6995 (10)	1106 (5)	7523 (11)	29
C(8)	10074 (11)	792 (4)	6195 (11)	23	C(29)	4837 (11)	1021 (4)	7240 (11)	28
C(9)	10980 (9)	1060 (4)	7075 (10)	16	C(30)	5659 (12)	1712 (5)	6729 (12)	31
C(10)	11576 (10)	1355 (4)	6374 (12)	24	O(31)	5936 (6)	819 (2)	2903 (7)	17
C(11)	11871 (10)	735 (4)	7380 (11)	21	C(32)	5485 (11)	507 (4)	1978 (10)	20
C(12)	10410 (11)	1311 (5)	7916 (12)	30	C(33)	4159 (11)	423 (4)	1818 (11)	23
O(13)	7781 (6)	1658 (2)	3978 (6)	11	C(34)	3445 (10)	828 (4)	1465 (12)	26
C(14)	8754 (10)	1912 (4)	3857 (10)	6	C(35)	3775 (11)	102 (4)	796 (11)	26
C(15)	8764 (11)	2344 (4)	4445 (10)	18	C(36)	3950 (11)	250 (4)	2993 (12)	28
C(16)	7680 (11)	2597 (4)	3845 (11)	22	O(37)	5035 (7)	1743 (3)	3184 (7)	19
C(17)	9840 (11)	2572 (4)	4259 (11)	23	C(38)	4157 (10)	2014 (4)	2383 (11)	20
C(18)	8857 (11)	2279 (4)	5807 (10)	21	C(39)	3352 (10)	2209 (4)	3101 (11)	22
O(19)	7917 (6)	1061 (2)	2585 (6)	15	C(40)	2747 (12)	1875 (4)	3640 (13)	31
C(20)	8123 (11)	804 (4)	1628 (11)	21	C(41)	2464 (12)	2477 (5)	2167 (13)	38
C(21)	9381 (10)	840 (4)	1523 (11)	24	C(42)	4079 (12)	2504 (4)	4071 (12)	28

Table II. Selected Bond Distances (Å) for $W_2(OCH_2$-t-$Bu)_6(\eta^2$-$C_2H_4)_2$ (1)

A	B	distance	A	B	distance
W(1)	W(2)	2.5331 (9)	W(2)	O(19)	2.323 (7)
W(1)	O(7)	1.892 (7)	W(2)	O(25)	2.317 (7)
W(1)	O(13)	2.282 (7)	W(2)	O(31)	1.999 (8)
W(1)	O(19)	2.004 (7)	W(2)	O(37)	1.885 (8)
W(1)	O(25)	1.991 (7)	W(2)	C(5)	2.146 (11)
W(1)	O(31)	2.312 (7)	W(2)	C(6)	2.151 (13)
W(1)	C(3)	2.127 (12)	C(3)	C(4)	1.451 (18)
W(1)	C(4)	2.137 (12)	C(5)	C(6)	1.447 (18)
W(2)	O(13)	1.977 (7)			

ligands are not contained in a plane. Alternatively expressed, the coordination geometry about the bridging oxygen atoms is distinctly pyramidal and not trigonal planar as is most commonly found.[14] The sum of the angles at oxygen are 338 (3)° (av). Taken together, the long W–O (bridging) distances and the pyramidal coordination at oxygen suggest weak and labile bridges. The structure may be viewed as the sum of two pseudotetrahedral $(RO)_3W(\eta^2$-$C_2H_4)$ moieties brought together to allow for M–M bonding as is schematically shown below.

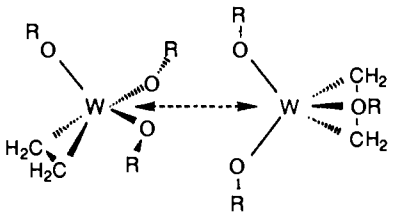

We have previously noted the complementary nature of carbonyl and alkoxide ligands and their many similar properties in polynuclear chemistry, e.g., fluxionality brought about by the opening and closing of bridges.[2,15] We have also noted that alkoxide ligands may adopt semibridging positions,[16] and in the structure of 1 the long W–O bridges are between a normal bridging distance and that of a semibridging distance. Given that $W_2(OR)_6L_2$ compounds, where L = a neutral σ donor ligand, adopt unbridged structures (eq 5), it is not unreasonable to propose that the bridged structure of 1 results from optimizing W d_π–C_2 π^* back bonding. This matter is discussed in detail later in this paper.

NMR Studies. We have previously described the ^1H and $^{13}C\{^1H\}$ NMR spectra of 1 which show the presence of three types of OCH_2-t-Bu ligands and four ethylenic ^1H signals as expected on the basis of a molecular structure with C_2 symmetry.[7,8b] The value of $^1J_{^{13}C-^{13}C}$ of 28 Hz is notably reduced from that of free ethylene, 67 Hz.[17] By use of the ethylene isotopomers *cis*-, *trans*-, and *gem*-$C_2H_2D_2$, we have also determined the ^1H–^1H coupling constants and their assignments. Since there are four nonequivalent H atoms per ethylene ligand and four multiplets in the ^1H NMR spectrum, the aforementioned study provided pairwise information such that the ABCD spin system could be assigned as in C below.

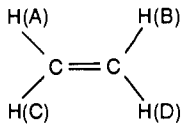

C

For reasons that will become apparent shortly, we determined that it would be useful to make an absolute assignment of the resonances H(A), H(B), H(C), and H(D) with respect to the ground-state structure and also assign the three sets of diastereotopic methylene protons of the neopentoxide ligands. By use of NOE difference spectroscopy between ethylenic and methylenic alkoxide protons and with knowledge of the H···H distances in the ground state, we were able to make the assignments shown in Figure 3 with a fair degree of confidence. NOE is an enhancement of the resonance of a proton that occurs when a proton close to it is irradiated. This is a through-space interaction, and it is roughly proportional to $1/r^6$, where r is the internuclear distance.[18] The assumption that the solution structure resembles the molecular structure seen in the solid-state X-ray crystallographic study and the observed NOE enhancements provide a self-consistent picture.

By ^1H–^1H decoupling experiments, we assigned the geminal pairs of methylenic protons [H(1), H(2)], [H(3), H(4)], and [H(5), H(6)] as shown in Figure 3. Of this set, only H(1) showed no NOE with any of the four ethylenic protons H(A), H(B), H(C), H(D). In the ground-state structure only one OC*H* bond is more than 2.6 Å from all of the ethylenic hydrogen atoms, and accordingly this was assigned H(1) as shown in Figure 3. Its geminal

(14) Bridging alkoxides use oxygen sp^2 hybrid orbitals and further oxygen p_π to metal d_π bonding may occur when the metal d_π orbitals of appropriate symmetry are vacant. Exceptions to trigonal-planar bridging oxygen atoms may arise for either electronic or steric reasons. For an unusual example of pyramidal coordination at oxygen in a bridging alkoxide, $Cp_2Cr_2(\mu$-O-t-Bu)$_2$, see: Chisholm, M. H.; Cotton, F. A.; Extine, M. W.; Rideout, D. C. *Inorg. Chem.* **1979**, *18*, 120.

(15) Buhro, W. E.; Chisholm, M. H. *Adv. Organomet. Chem.* **1987**, *27*, 311.

(16) Chisholm, M. H.; Folting, K.; Huffman, J. C.; Kirkpatrick, C. C. *J. Chem. Soc., Chem. Commun.* **1982**, 188.

(17) Stothers, J. B. *Carbon-13 NMR Spectroscopy*; Academic Press: New York, 1972; p 327, Table 9.3.

(18) Derome, A. E. *Modern NMR Techniques for Chemistry Research*; Pergamon Press: Oxford, 1987; Ch. 5.

Table III. Selected Bond Angles for $W_2(OCH_2\text{-}t\text{-}Bu)_6(\eta^2\text{-}C_2H_4)_2$ (**1**)

A	B	C	angle (deg)	A	B	C	angle (deg)	A	B	C	angle (deg)
W(2)	W(1)	O(7)	129.16 (22)	O(31)	W(1)	C(3)	84.4 (4)	O(31)	W(2)	O(37)	107.5 (3)
W(2)	W(1)	O(13)	48.13 (17)	O(31)	W(1)	C(4)	87.0 (4)	O(31)	W(2)	C(5)	93.5 (4)
W(2)	W(1)	O(19)	60.25 (20)	C(3)	W(1)	C(4)	39.8 (5)	O(31)	W(2)	C(6)	129.2 (4)
W(2)	W(1)	O(25)	60.20 (20)	W(1)	W(2)	O(13)	59.28 (20)	O(37)	W(2)	C(5)	97.0 (4)
W(2)	W(1)	O(31)	48.46 (19)	W(1)	W(2)	O(19)	48.50 (18)	O(37)	W(2)	C(6)	98.1 (4)
W(2)	W(1)	C(3)	129.9 (4)	W(1)	W(2)	O(25)	48.23 (17)	C(5)	W(2)	C(6)	39.4 (5)
W(2)	W(1)	C(4)	131.5 (4)	W(1)	W(2)	O(31)	59.99 (21)	W(1)	O(7)	C(8)	131.7 (7)
O(7)	W(1)	O(13)	81.0 (3)	W(1)	W(2)	O(37)	128.96 (22)	W(1)	O(13)	W(2)	72.59 (22)
O(7)	W(1)	O(19)	107.5 (3)	W(1)	W(2)	C(5)	130.8 (5)	W(1)	O(13)	C(14)	127.7 (6)
O(7)	W(1)	O(25)	107.8 (3)	W(1)	W(2)	C(6)	129.1 (4)	W(2)	O(13)	C(14)	136.5 (6)
O(7)	W(1)	O(31)	177.4 (3)	O(13)	W(2)	O(19)	69.83 (27)	W(1)	O(19)	W(2)	71.25 (22)
O(7)	W(1)	C(3)	97.5 (4)	O(13)	W(2)	O(25)	69.30 (25)	W(1)	O(19)	C(20)	134.0 (7)
O(7)	W(1)	C(4)	95.6 (4)	O(13)	W(2)	O(31)	119.2 (3)	W(2)	O(19)	C(20)	134.5 (7)
O(13)	W(1)	O(19)	70.27 (27)	O(13)	W(2)	O(37)	108.3 (3)	W(1)	O(25)	W(2)	71.57 (21)
O(13)	W(1)	O(25)	69.82 (27)	O(13)	W(2)	C(5)	128.0 (4)	W(1)	O(25)	C(26)	134.2 (7)
O(13)	W(1)	O(31)	96.58 (25)	O(13)	W(2)	C(6)	91.5 (4)	W(2)	O(25)	C(26)	129.2 (6)
O(13)	W(1)	C(3)	160.2 (4)	O(19)	W(2)	O(25)	96.71 (25)	W(1)	O(31)	W(2)	71.55 (23)
O(13)	W(1)	C(4)	159.8 (4)	O(19)	W(2)	O(31)	72.26 (28)	W(1)	O(31)	C(32)	134.8 (7)
O(19)	W(1)	O(25)	120.4 (3)	O(19)	W(2)	O(37)	177.28 (28)	W(2)	O(31)	C(32)	134.1 (7)
O(19)	W(1)	O(31)	72.41 (27)	O(19)	W(2)	C(5)	85.7 (4)	W(2)	O(37)	C(38)	130.5 (7)
O(19)	W(1)	C(3)	128.2 (4)	O(19)	W(2)	C(6)	83.9 (4)	W(1)	C(3)	C(4)	70.5 (7)
O(19)	W(1)	C(4)	92.2 (4)	O(25)	W(2)	O(31)	70.11 (27)	W(1)	C(4)	C(3)	69.7 (7)
O(25)	W(1)	O(31)	70.33 (27)	O(25)	W(2)	O(37)	80.7 (3)	W(2)	C(5)	C(6)	70.5 (7)
O(25)	W(1)	C(3)	92.2 (4)	O(25)	W(2)	C(5)	161.6 (4)	W(2)	C(6)	C(5)	70.1 (7)
O(25)	W(1)	C(4)	129.6 (4)	O(25)	W(2)	C(6)	159.0 (4)				

Table IV. Summary of Crystal Data for $W_2(OCH_2\text{-}t\text{-}Bu)_6(\eta^2\text{-}C_2H_4)_2$ (**1**)

empirical formula	$W_2C_{34}H_{74}O_6$
color of crystal	yellow
crystal dimensions (mm)	0.15 × 0.20 × 0.20
space group	$P2_1/c$
cell dimensions	
temp (°C)	−155
a (Å)	11.754 (4)
b (Å)	31.405 (14)
c (Å)	11.274 (4)
β (deg)	104.96 (2)
Z (molecules/cell)	4
volume (Å^3)	4020.77
calcd density (gm/cm^3)	1.564
λ (Å)	0.71069
mol wt	946.65
linear absorption coeff (cm^{-1})	58.757
detector to sample distance (cm)	22.5
sample to source distance (cm)	23.5
average ω scan width at half height	0.25
scan speed (deg/min)	6.0
scan width (deg + dispersion)	1.5
individual background (s)	6
aperture size (mm)	3.0 × 4.0
2θ range (deg)	6–45
total no. of reflections collected	5494
no. of unique intensities	5274
no. with $F > 0.0$	4908
no. with $F > 2.33\sigma(F)$	4412
$R(F)$	0.0430
$Rw(F)$	0.0418
goodness of fit for last cycle	0.951
maximum δ/σ for last cycle	0.35

Table V. Structural and NMR Spectroscopic Parameters of Early Transition Metal Ethylene Complexes and Related Compounds

compound	$d_{C\text{-}C}$ (Å)	$J_{^{13}C\text{-}^{13}C}$ (Hz)
C_2H_4	1.339[1]	67[17]
$(C_5H_5)_2Nb(C_2H_5)(\eta^2\text{-}C_2H_4)$	1.406 (13)[a]	
$[MoH(OOCCH{=}CH_2)(\eta^2\text{-}C_2H_4)(PMe_3)_2]_2$	1.426 (9)[b]	
$[WH(OOCCH{=}CH_2)(\eta^2\text{-}C_2H_4)(PMe_3)_2]_2$	1.443 (2)[b]	
$W_2(O\text{-}i\text{-}Pr)_6(CH_2)_4(\eta^2\text{-}C_2H_4)$	1.43 (2)[7]	25[7]
$W_2(OCH_2\text{-}t\text{-}Bu)_6(\eta^2\text{-}C_2H_4)_2$	1.45 (2)[c]	28[7]
$W_2(C_2H_5)(O\text{-}c\text{-}C_5H_9)_7(\eta^2\text{-}C_2H_4)$	1.46 (3)[d]	35[d]
$(\eta^5\text{-}C_5Me_5)Ta(CHCMe_3)(\eta^2\text{-}C_2H_4)(PMe_3)$	1.477 (4)[e]	
$[Li(tmed)]_2[Hf(C_2H_5)_4(\eta^2\text{-}C_2H_4)]$	1.51[f]	
$Ti(C_2H_4)Me_2(\eta^2\text{-dmpe})(\eta^1\text{-dmpe})$		39[f]
$(ArO)_2Ti(\eta^2\text{-}C_2H_4)(PMe_3)$	1.425 (3)[g]	
C_2H_6	1.538 (2)[11]	34.6[17]

[a] Guggenberger, L. J.; Meakin, P.; Tebbe, F. N. *J. Am. Chem. Soc.* **1974**, *96*, 5420. [b] Alvarez, R.; Carmona, E.; Galindo, A.; Gutiérrez, E.; Marin, J. M.; Monge, A.; Poveda, M. L.; Ruiz, C.; Savariault, J. M. *Organometallics* **1989**, *8*, 2430. [c] This work. [d] Chacon, S. T.; Chisholm, M. H.; Streib, W. E., results to be published. [f] Girolami, G. S., result to be published. These examples have a d^2 metal center which is similar to $W_2(OCH_2\text{-}t\text{-}Bu)_6(\eta^2\text{-}C_2H_4)_2$ (**1**), which has a W–W single bond, leaving each metal center with two d electrons for bonding to the η^2-C_2H_4 ligand. [g] Hill, J. E.; Fanwick, P. E.; Rothwell, I. P. Organometallics. In press. ArO = 2,6-diphenylphenoxide. This example also has a d^2 metal center.

Table VI. Nuclear Overhauser Enhancement and Distances between Ethylenic and Methylenic Protons of $W_2(OCHD\text{-}t\text{-}Bu)_6(\eta^2\text{-}C_2H_4)_2$ (**1**-d_6), Obtained at −20 °C in CD_2Cl_2

O–CH_2 proton	C_2H_4 proton	distance (Å)	NOE (%)[a]
H(1)		>2.6	
H(2)	H(C)	2.3	6
H(3)	H(A)	2.4	6
H(4)	H(B)	2.3	5
H(5)	H(D)	2.3	6
H(6)	H(D)	2.2	12

[a] % NOE was determined in relationships to the irradiated signal as −100%.

proton, H(2), showed NOE with the ethylenic H(C). Since the closest ethylenic H atom to H(2) is at a distance of 2.3 Å, we assign the resonance as shown in Figure 3.

The maximum NOE[19] is seen between H(6) and the ethylenic resonance H(D). The short H···H distance in the ground-state structure leads to the assignment of H(6) and olefinic H(D) as shown in Figure 3. Two predictions can now be checked, and both are found to be consistent with the above assignment of H(6) and H(D): (1) H(5) and H(6) are geminal protons and H(5) shows NOE to the other ethylenic H(D) proton and (2) from knowledge of the ethylenic couplings we know that H(D) is cis to H(C). We have now an internally consistent assignment for the methylenic protons H(1), H(2), H(5), and H(6) and the ethylenic protons H(C) and H(D). By similar NOE difference measurements the assignment of H(3) and H(4) was made, and in each instance the

(19) This discussion concerns NOE between the ethylenic and methylenic alkoxide protons, as stated in the text. The NOE between geminal sets of protons is greater, as noted in the Experimental Section.

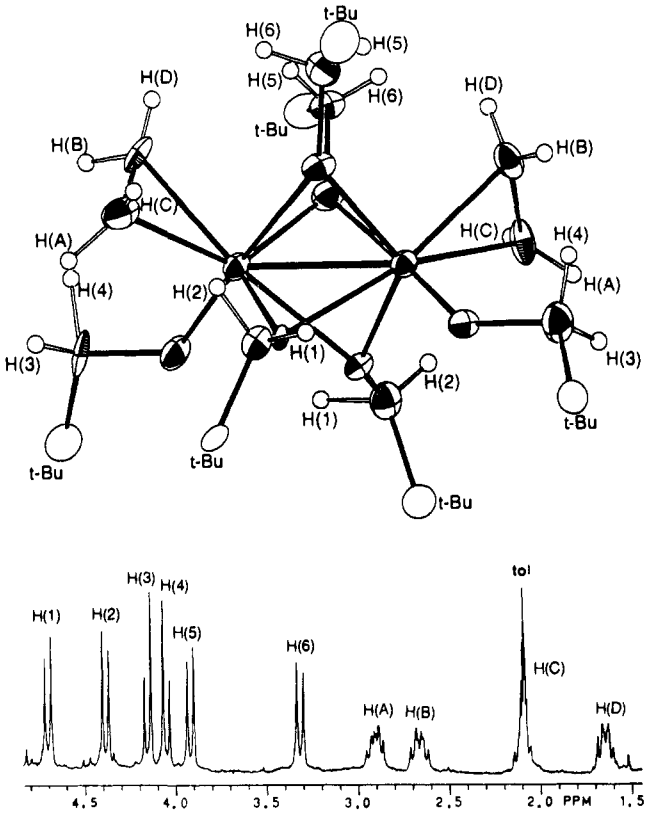

Figure 3. ^{1}H NMR of $W_2(OCH_2$-*t*-**Bu**$)_6(\eta^2$-$C_2H_4)_2$ (**1**) in toluene-d_8 at 15 °C, showing the methylenic alkoxide protons as doublets labeled H(1)–H(6) and the ethylenic protons as multiplets labeled H(A)–H(D), one partially obscured by the protio impurity of the NMR solvent. The assignments are shown on the accompanying ORTEP diagram. The *t*-Bu groups of the neopentoxide ligands are indicated as large circles. The methylenic alkoxide protons and ethylenic protons are small circles.

correlation with ethylenic H atoms remained consistent. There was no observed NOE between H atoms that were more than 2.5 Å apart in the ground-state molecular structure. In every instance of an estimated H···H distance of 2.4 Å or less, NOE was observed. The data are summarized in Table VI.

Investigations of the dynamic behavior of **1** were limited by the equilibrium 4 such that olefin rotation, for example, could not be detected by line broadening. Furthermore, when an excess of ethylene was added to favor the presence of **1** in equilibrium 4 at higher temperatures, wherein W–C_2 rotation might be expected to be rapid (NMR timescale), the further reactions shown in Scheme I became dominant. However, by the use of spin saturation transfer (SST) difference spectroscopy[20] we were able to monitor the dynamic behavior of **1** in the temperature range of 5–25 °C.

In order to eliminate the NOE between the geminal methylenic protons of the neopentoxy ligands, we prepared the labeled compound $W_2(OCHD$-*t*-$Bu)_6(\eta^2$-$C_2H_4)_2$. In this way the SST difference spectrum is not perturbed by any unwanted NOE.

The results of these NMR studies are really rather interesting and somewhat unexpected. First, as we show in Figure 4, the ethylenic protons are undergoing site exchange in a pairwise manner, and the pairwise exchange involves the cis hydrogen atoms: H(A) ⇄ H(B) and H(C) ⇄ H(D).[20] In Figure 4, the small enhancement of the geminal ethylenic signals is due to NOE which we have not eliminated by deuterium labeling (c.f., the use of OCHD-*t*-Bu ligands).

The SST difference spectra for the methylenic hydrogen atoms of the neopentoxide ligands are shown in Figure 5. From this we see that *one* geminal pair (H(5,6)) undergoes self-exchange.

(20) Sandström, J. *Dynamic NMR Spectroscopy*; Academic Press: New York, 1982; Ch. 4. In the difference spectrum, the irradiated proton gives a fully negative signal. A dynamic site exchange involving this hydrogen atom will cause a negative signal for the other proton involved in the exchange.

Figure 4. ^{1}H NMR SST difference studies of the ethylenic protons of $W_2(OCHD$-*t*-$Bu)_6(\eta^2$-$C_2H_4)_2$ (**1**) in CD_2Cl_2 at 15 °C. The top spectrum shows the four multiplets arising from ethylenic protons. Other peaks come from further reaction with ethylene as in Scheme I. The difference spectra shown below indicate exchange between H(A) ⇄ H(B) and H(C) ⇄ H(D). Positive peaks are caused by NOE.

These CH bonds are associated with the alkoxide bridges trans to the terminal alkoxide ligands. The fact that we observed H(1) ⇄ H(4) and H(2) ⇄ H(3) indicates a selective site exchange between different geminal pairs. The only possible explanation for this is bridge ⇄ terminal exchange involving the bridging alkoxide that is trans to the olefin. From a close inspection of Figure 5, one can see some small magnetization transfer between all six methylene H atoms. We believe that this results from a slower but still significant exchange involving equilibrium 4. Consistent with this, we have observed some magnetization transfer between free ethylene and the coordinated ethylene in **1** at 20 °C.

These observations lead us to propose that compound **1** undergoes an enantiomerization by way of the process shown in eq 7. The activated complex [**1***] is proposed to have an edge-shared

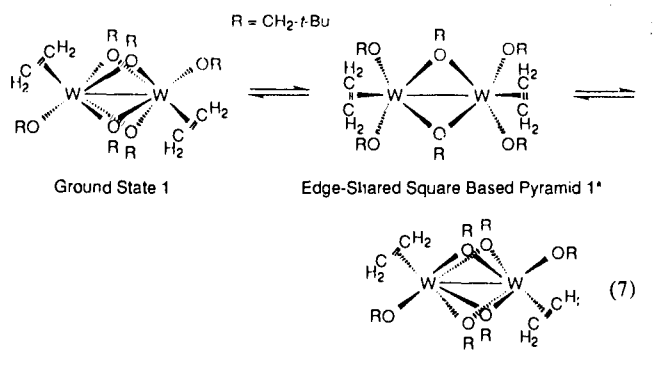

(7)

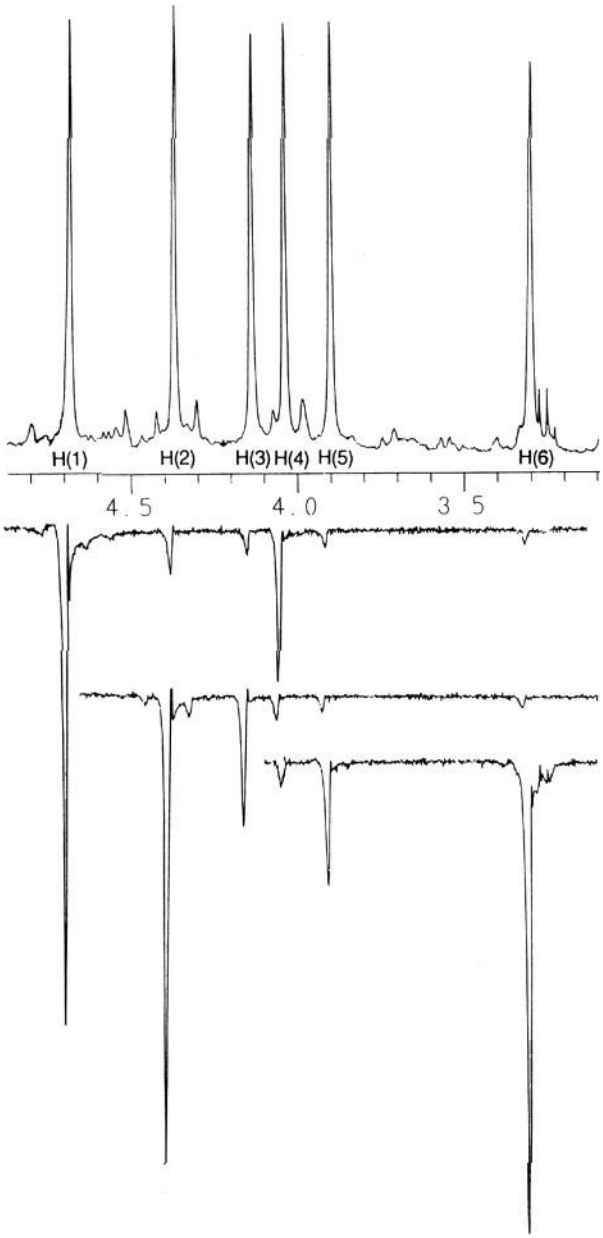

Figure 5. ^{1}H NMR SST difference studies of the methylenic protons of the alkoxides of $W_2(OCHD\text{-}t\text{-}Bu)_6(\eta^2\text{-}C_2H_4)_2$ (**1**-d_6). The top spectrum shows the six singlets due to the methylenic alkoxide protons, which are no longer doublets as in Figure 3 due to deuterium substitution. Other peaks come from further reaction products as shown in Scheme I. The difference spectra below show exchange between H(1) ⇄ H(4), H(2) ⇄ H(3), and H(5) ⇄ H(6).

Table VII. Kinetic Data for the Fluxional Process Involving $W_2(OCH_2\text{-}t\text{-}Bu)_6(\eta^2\text{-}C_2H_4)_2$ (**1**)

T (°C) ± 1	k (s^{-1})	T_1 (s)[a]	SST (%)[b]
5	0.20	0.29 ± 0.01	5.5
10	0.39	0.29 ± 0.03	10.1
15	0.65	0.33 ± 0.01	17.7
20	0.91	0.37 ± 0.01	25.3
23	1.1	0.384 ± 0.002	30.0
25	1.4	0.39 ± 0.01	35.7

[a] T_1 = longitudinal or spin–lattice relaxation time. [b] SST = spin saturation transfer. The % is determined in relationship to the irradiated signal as 100%.

square-based pyramidal geometry. Again the olefinic C_2 axis is perpendicular to the W–W axis and occupies an apical site of the square-based pyramid. This geometry for the activated complex

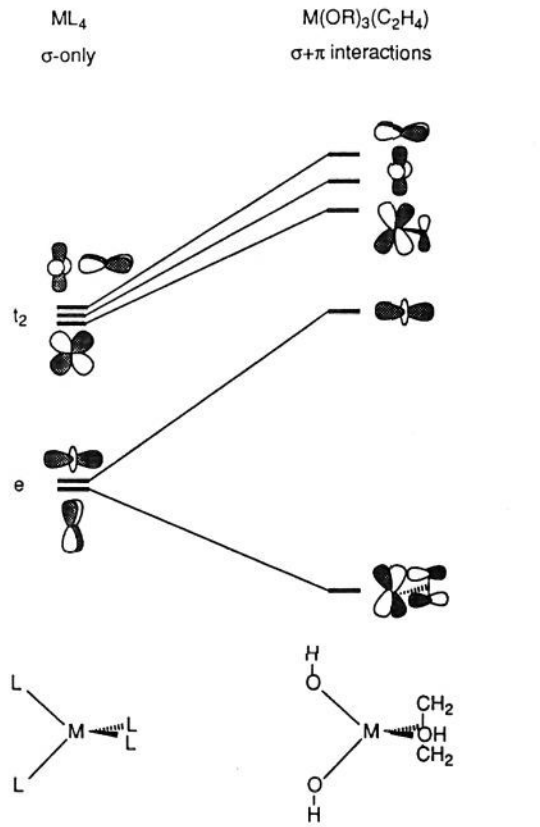

Figure 6. Qualitative molecular orbital diagram for the d orbital splitting in $M(OR)_3(\eta^2\text{-}C_2H_4)$ starting with tetrahedral symmetry on the left and then including the π interactions of the ethylene π^* and oxygen p orbitals on the right.

contains two mirror planes of symmetry and a C_2 axis. H(6) and H(5), the geminal protons, are equivalent as are the ethylenic protons that are mutually cis, H(A) ⇄ H(B) and H(C) ⇄ H(D). The other methylenic protons are diastereotopic, and by the reversible opening and closing of bridges as shown in eq 7, we attain the selective exchange H(1) ⇄ H(4) and H(2) ⇄ H(3).

From the SST studies in the temperature range 5–25 °C, we have been able to obtain activation parameters for this fluxional process. The Arrhenius plot is shown in the supplementary material, and the kinetic data are shown in Table VII. This gives $\Delta G^\ddagger = 14.08 \pm 0.9$ kcal mol^{-1}, $\Delta H^\ddagger = 13.4 \pm 0.9$ kcal mol^{-1}, and $\Delta S^\ddagger = -13 \pm 3$ cal K^{-1} mol^{-1}. Thus, the barrier to ethylene–tungsten bond rotation in **1** must have $\Delta G^\ddagger > 14$ kcal mol^{-1}, and this is an indirect measure of the W d_π–C_2 π^* back bonding as will become evident from the considerations of bonding which follow.

Bonding Considerations and Theoretical Analysis. A simple understanding of the qualitative features of the bonding can be obtained on the basis of the view that **1** is the sum of two d^3-$W(OR)_3(\eta^2\text{-}C_2H_4)$ pseudotetrahedral moieties. The splitting of the d orbitals in T_d symmetry is t_2 and e, where the e set is not used in metal–ligand σ bonding but is available for π bonding. The presence of the single face π-acceptor ligand C_2H_4 will remove the degeneracy of the e d_π orbitals. One of the d_{z^2} or $d_{x^2-y^2}$ orbitals will then π-bond with the olefin and thus become stabilized. With the alkoxide-filled oxygen p_π orbitals, the other t_2 and d_{z^2} orbitals will be raised in energy. This simple splitting pattern of one below four with the d_{z^2} orbitals still below the t_2 set is shown in Figure 6. The selection of the coordinate system shown allows for the formation of an M–M σ bond upon bringing two d^3-$W(OH)_3$-$(\eta^2\text{-}C_2H_4)$ fragments together as shown in Figure 7.

The simple pictorial model is supported by the calculations employing the method of Fenske and Hall[21] on the hypothetical

(21) Hall, M. B.; Fenske, R. F. *Inorg. Chem.* **1972**, *11*, 768.

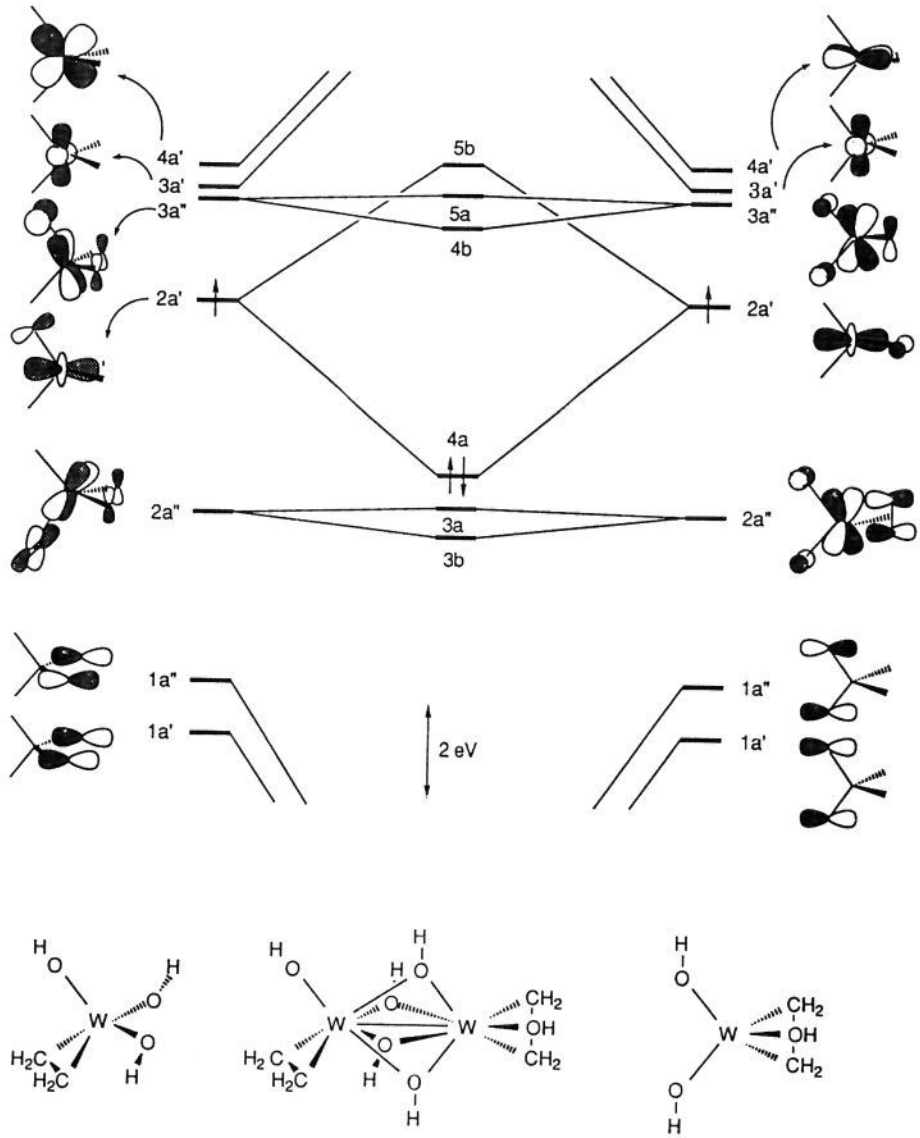

Figure 7. Frontier molecular orbital diagram of $W_2(OH)_6(\eta^2\text{-}C_2H_4)_2$, viewed as the sum of two pseudotetrahedral $d^3\text{-}W(OH)_3(\eta^2\text{-}C_2H_4)$ fragments.

fragment $d^3\text{-}W(OH)_3(\eta^2\text{-}C_2H_4)$ and molecule $W_2(OH)_6(\eta^2\text{-}C_2H_4)_2$. The HOMO is the M–M σ bonding molecular orbital formed from the overlap of two d_{z^2} atomic orbitals. The LUMO is a metal-centered δ^* orbital. The orbitals directly below the HOMO, orbitals 3a and 3b in Figure 7, are predominantly tungsten d_π–ethylene π^* bonding with a small admixture of oxygen p_π from a pair of bridging OH ligands. In the ground-state structure of **1**, it is the mutual competition between M–M σ bonding and M–C_2 π^* back bonding that causes the specific alignment of the C_2 axes as shown in Figure 2. The C_2 axes must be perpendicular to the W–W axis for the molecule to form an M–M σ bond. If the C_2 axes are rotated by 90°, then W d_π–C_2 π^* back bonding utilizes the W d_{z^2} orbital and the M–M bonding would involve the δ-type orbitals which leads to poor M–M overlap and ineffective M–M bonding. Mixing of the M–M δ orbitals with the oxygen p_π orbitals causes the M–M δ^* orbital to be lower in energy than the M–M δ orbital so that the HOMO in Figure 8 is calculated to be M–M δ^*. Therefore, rotation of the ethylene ligand by 90° causes the M–M bonding to change from M–M σ bonding to M–M δ antibonding. From inspection of Figure 8 we can see that W–C_2 olefin rotation is not only enthalpically disfavored but also a symmetry-forbidden process.

The Asymmetric Ligand Bridges. As noted earlier, the central W_2O_4 core contains asymmetric W–O bonds, four short (2.00 (1) Å) and four long (2.31 (1) Å), and each bridging oxygen is pyramidal and most distinctly not trigonal planar as is most often seen for bridging alkoxides. One may take the view that the coordination about each tungsten atom is largely determined by W d_π–C_2 π^* bonding and the formation of an M–M σ bond, and thus the joining of two $d^3\text{-}W(OR)_3(\eta^2\text{-}C_2H_4)$ tetrahedral fragments will of necessity introduce incidental metal–ligand contacts as shown below in D. This accounts for the presence of two long

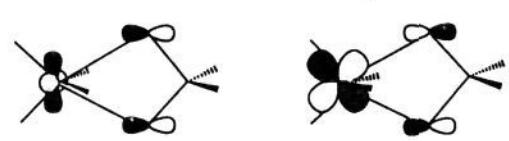

D

W–OR bridges to each tungsten atom. Alternatively, one might consider that the long bonds result from the trans influence of the trans C_2H_4 and terminal OR ligands. Since the bridges are asymmetric to the same extent, the trans influence of ethylene and alkoxide would be comparable.[22] To our knowledge, the relative trans influence order of ethylene and OR ligands has not

(22) Appleton, T. G.; Clark, H. C.; Manzer, L. M. *Coord. Chem. Rev.* **1973**, *10*, 335.

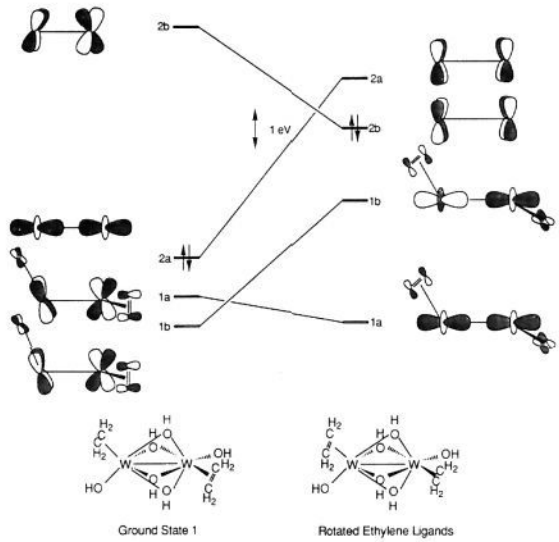

Figure 8. Walsh diagram from the results of Fenske–Hall calculations for the frontier MOs of $W_2(OH)_6(\eta^2\text{-}C_2H_4)_2$ with the geometry of **1** for the rotation of the ethylene ligands. The rotation is forbidden if C_2 symmetry is preserved and the metal coordination geometry is maintained.

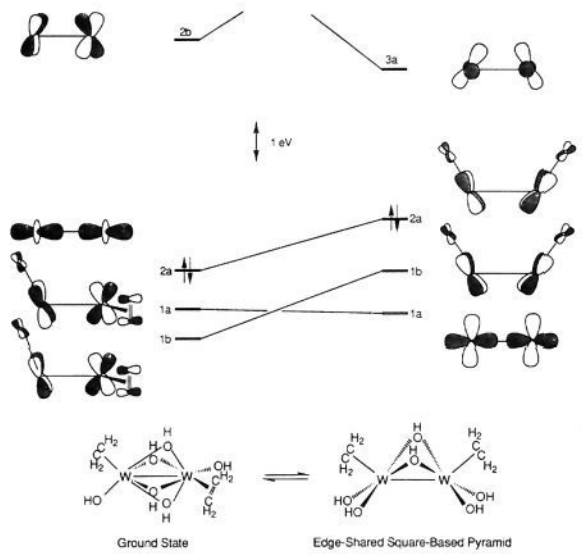

Figure 9. Walsh diagram from the results of Fenske–Hall calculations for the frontier MOs of $W_2(OH)_6(\eta^2\text{-}C_2H_4)_2$ for the skeletal rearrangement: ground-state structure to edge-shared square-based pyramid. The rearrangement is symmetry-allowed and leads to a higher energy structure.

been previously established, and because of this we considered this matter further.

The following trans influence order has been established previously: CO ≥ RNC ≥ C=C ≥ Cl^- ≥ NH_3 > O(acac) for a variety of metal centers with differing oxidation states and geometries.[22] Inspection of the structures $Mo(O\text{-}i\text{-}Pr)_2(bpy)_2$[23] and $Mo(bpy)_2(CO)_2$[24] would suggest that alkoxide would join the series as CO > OR > bpy.[25] Thus, it is quite possible that ethylene and alkoxide could have comparable trans influence, especially when it is considered that both ligands should be capable of exhibiting a variable trans influence. Both ligands are π-buffers, and the strength of the σ bond is affected by the extent of π bonding. The anion $[V_2(edt)_4]^{2-}$ (edt = ethylenedithiolate) has a similar skeletal structure with less pronounced asymmetry of the bridging ligands.[26] That might lead one to believe that thiolate ligands have a weaker trans influence than alkoxide ligands, which is supported by inspection of the structures $[V(SC_6H_5)_2(C_{10}N_2H_8)_2]^+$,[27] $[VO(SPh)_3(bpy)]^-$,[27] $[VO(SPh)_3(Me_2bpy)]^-$,[27] $Sn(SPh)_4bpy$,[28] and $Ni(bpy)_2(SPh)_2$[29] and leads to the trans influence series: OR > SR ≥ bpy.

Extended Hückel (EHT) calculations[30] were carried out on the model $W_2(OH)_6(\eta^2\text{-}C_2H_4)_2$ system *in which all bridges were symmetric*. The calculation showed the W–O overlap population for the bridging hydroxide trans to the ethylene ligands (0.24) to be smaller than that for the other three bridging hydroxide ligands (0.26), one of which is trans to the terminal hydroxide ligand. Fenske–Hall calculations showed analogous results with corresponding overlap populations of 0.23 and 0.27. Since the calculations revealed that rotation of the olefin by 90° did not change the W–O overlap populations, the asymmetry is associated with the M–ethylene σ bond in agreement with our above discussion. The calculations did not show a decrease in overlap populations for the bridging ligands trans to the terminal hydroxide ligands. In our belief, this is due to the intrinsic difficulty of calculations to reproduce the σ bond strength.[31]

Further calculations were carried out on the model system $W_2(OH)_6(\eta^2\text{-}C_2H_4)_2$. The bond lengths of the two bridging hydroxide ligands trans to the terminal hydroxide ligands were varied to be either symmetrical or asymmetrical as in the ground-state structure. The total energy of the ground-state structure was 18 kcal/mol lower than the structure with two symmetrically bridging ligands (from EHT results). Examination of the MOs show that the stabilization is dispersed over several orbitals. Although such results should be taken with caution, the stabilization appears to be significant.

Theoretical Investigations Relating to the Dynamic Behavior of 1 and the Coupling of Two Ethylene Ligands at the Dinuclear Center. As noted earlier, compound **1** displays fluxional behavior in solution, and our NMR studies lead us to propose that bridges reversibly open to give a molecule having C_{2v} symmetry and a single pair of OR bridges. (See eq 7.) We have investigated the bonding in a hypothetical molecule $W_2(\mu\text{-}OH)_2(OH)_4(\eta^2\text{-}C_2H_4)_2$ having C_{2v} symmetry in an idealized edge-shared square-based pyramid. (Distances and angles are given in the Experimental Section under Computational Procedures and were based on our knowledge of the structure of **1**.) The frontier MOs for the ground-state and the proposed activated complex are shown in Figure 9. The calculations suggest that in the C_{2v} geometry, the frontier orbitals are raised in energy. However, in C_2 symmetry, the proposed opening and closing of bridges (eq 7) is a symmetry-allowed process.

In considering alternate structures such as the C_{2v} intermediate shown in eq 7, we were struck by the similar structure observed

(23) Chisholm, M. H.; Huffman, J. C.; Rothwell, I. P.; Bradley, P. G.; Kress, N.; Woodruff, W. H. *J. Am. Chem. Soc.* **1981**, *103*, 4945.
(24) Chisholm, M. H.; Connor, J. A.; Huffman, J. C.; Kober, E. M.; Overton, C. *Inorg. Chem.* **1984**, *23*, 2298.
(25) Here a comparison is made based on Mo–N distances involving trans CO and OR ligands. The mutually trans Mo–N distances are the same in $Mo(O\text{-}i\text{-}Pr)_2(bpy)_2$ and $Mo(CO)_2(bpy)_2$ despite the difference in oxidation states of the Mo atoms.
(26) (a) Szeymies, D.; Krebs, B.; Henkel, G. *Angew. Chem., Int. Ed. Engl.* **1983**, *22*, 885. (b) Wiggins, R. W.; Huffman, J. C.; Christou, G. *J. Chem. Soc., Chem. Commun.* **1983**, 1313. (c) Dorfman, J. R.; Holm, R. H. *Inorg. Chem.* **1983**, *22*, 3179.
(27) Christou, G.; Dean, N. S.; Huffman, J. C.; Streib, W. E., results to be published.
(28) Hencher, J. L.; Khan, M.; Said, F. F.; Sieler, R.; Tuck, D. G. *Inorg. Chem.* **1982**, *21*, 2787.
(29) Osakada, K.; Yamamoto, T.; Yamamoto, A.; Takenaka, A.; Sasada, Y. *Acta Crystallogr.* **1984**, *C40*, 85.
(30) Weighted H_{ij} formula: Ammeter, J. H.; Bürgi, H.-B.; Thibeault, J. C.; Hoffmann, R. *J. Am. Chem. Soc.* **1978**, *100*, 3686. W parameters: Dedieu, A.; Albright, T. A.; Huffmann, R. *J. Am. Chem. Soc.* **1979**, *101*, 3141.
(31) This difficulty can be found at all levels of calculations. For instance, even ab initio calculations do not easily account for the problem of cis/trans isomers of formula $M(CO)_4L_2$ and $M(CO)_4(L)(L')$ where L = a neutral donor amine or tertiary phosphine and M = Cr or Mo: Daniel, C.; Veillard, A. *Inorg. Chem.* **1989**, *28*, 1170.

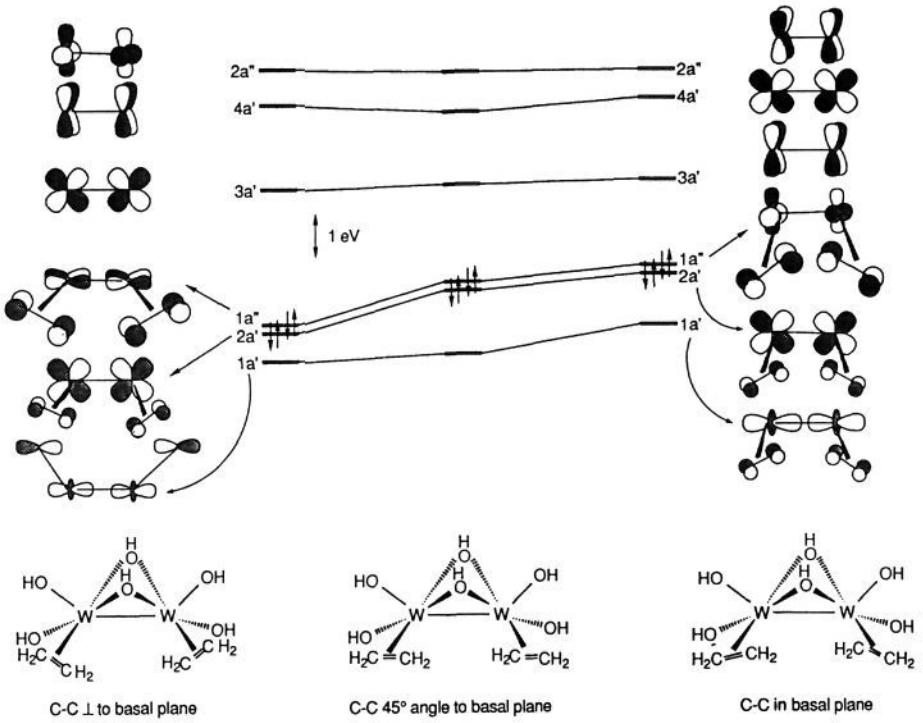

Figure 10. Walsh diagram from the results of Fenske–Hall calculations for the frontier MOs of $W_2(OH)_6(\eta^2\text{-}C_2H_4)_2$ in a square-based bipyramidal geometry with basal ethylene ligands for the rotation of the ethylene ligands. C_s symmetry is maintained and the process is symmetry-allowed.

for $W_2(CH_2Ph)_2(O\text{-}i\text{-}Pr)_4(\eta^2\text{-}C_2Me_2)_2$.[32] This is schematically depicted by E below.

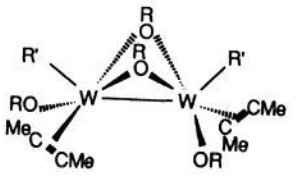

E

The molecule has C_2 symmetry, and each tungsten atom is in a square-based pyramidal coordination environment. The two tungsten atoms are joined along a common basal edge by the two bridging alkoxide ligands, and the benzyl groups occupy the apical positions. The C_2 axis of the alkyne is perpendicular to the basal plane. The presence of the strong σ-donor benzyl ligand in the apical site and the π-acceptor alkyne in the basal position is in agreement with the predictions of site occupancies in square-pyramidal geometries that have been forwarded by Rossi and Hoffmann.[33] This led us to consider an analogous structure for a hypothetical $W_2(\mu\text{-}OH)_2(OH)_4(\eta^2\text{-}C_2H_4)_2$ molecule. Calculations indicate that such a structure is quite acceptable, and indeed the HOMO is lower in energy than when the ethylene is in the apical position. Thus, if an edge-shared square-based bipyramidal structure were the ground state, then we would expect to see this similarity with the $W_2(CH_2Ph)_2(O\text{-}i\text{-}Pr)_4(\eta^2\text{-}C_2Me_2)_2$ molecule. In this type of structure there should be a relatively low barrier to olefin rotation as shown in Figure 10. In the case of the alkyne adducts, the barrier to W–C_2–alkyne rotation, $\Delta G^{\ddagger}$, fell in the range of 9–14 kcal mol^{-1} and was observed by ^{1}H NMR coalescence of the alkynyl substituent RCCR′, where R = Me and R′ = Me and Et. The higher barriers were observed for supporting *t*-BuO ligands compared to *i*-PrO ligands, which suggests that the actual electronic barrier to alkyne rotation is less than 9 kcal mol^{-1}. One must ask why the observed structure is favored relative to the analogous alkyne structure just described (E). The nature of our calculational methods does not allow meaningful absolute energies to be calculated although the trends in relative energies are usually reliable. There are perhaps two things that appear to disfavor the structure of type E relative to that observed. (1) The HOMO–LUMO gap is somewhat smaller in the former—roughly one-half as large as that calculated for **1**. (2) The HOMO and SHOMO, 1a″ and 2a′ in Figure 10, are metal–ligand bonding molecular orbitals, principally W d_π–C π^* in character. The M–M σ bonding orbital, 1a′, lies below both, whereas in the calculation on $W_2(\mu\text{-}OH)_4(OH)_2(\eta^2\text{-}C_2H_4)_2$ (based on the ground state structure of **1**) we see that the order is reversed. The HOMO is the M–M σ, and below this are the W d_π–C_2 π^* bonding molecular orbitals. In general it can be stated that metal–ligand bonding is more important (i.e., stronger) than metal–metal bonding, and calculations in organometallic and metalloorganic cluster chemistry repeatedly find that the HOMO is M–M bonding and not M–L bonding.[34]

After discussing these various structures for an activated $W_2(OCH_2\text{-}t\text{-}Bu)_6(\eta^2\text{-}C_2H_4)_2$ molecule, we must stress that the structure analogous to E is *alone* an unacceptable intermediate or activated complex in the observed fluxional process. In the absence of W–C_2 bond rotation, all four ethylenic hydrogen atoms are inequivalent. If rotation is facile, as has been suggested for such a species (Figure 10 and by analogy with the alkyne adducts), then there would be a selective pairwise site exchange of trans protons rather than the observed cis site exchange. The proposed fluxional process, that shown in eq 7, is sufficient to explain the NMR observations.

Concerning the Nature of Metallacycle Formation. We spent considerable time attempting to determine the role of compound **1** in the formation of the metallacycle–ethylene complex shown in Scheme I. We carried out NMR studies employing ^{13}C-substituted ethylene ($^{13}C^{12}CH_4$) wherein three sets of reactions were followed by ^{13}C NMR spectroscopy at various temperatures: (a) $W_2(OCH_2\text{-}t\text{-}Bu)_6(\eta^2\text{-}C_2H_4)_2 + {}^{13}CCH_4$, (b) $W_2(OCH_2\text{-}t\text{-}Bu)_6(\eta^2\text{-}{}^{13}CCH_4)_2 + C_2H_4$, and (c) $W_2(OCH_2\text{-}t\text{-}Bu)_6(\eta^2\text{-}{}^{13}CCH_4)_2 +$

(32) (a) Chisholm, M. H.; Eichhorn, B. W.; Folting, K.; Huffman, J. C. *Organometallics* **1989**, *8*, 49. (b) A closely related structure involving an edge-shared square-based pyramid was also seen in the η^2-aldehyde (η^2-O-C) adducts $W_2(OCH_2\text{-}t\text{-}Bu)_6(\eta^2\text{-}OCHCHCHMe)_2$: Chisholm, M. H.; Lucas, E. A.; Sousa, A. C.; Huffman, J. C. *J. Chem. Soc., Chem. Commun.* **1991**, 847.

(33) Rossi, A. R.; Hoffmann, R. *Inorg. Chem.* **1975**, *14*, 365.

(34) Bursten, B. E., personal communication.

$^{13}CCH_4$. The latter reaction provided a blank. The use of the mono-^{13}C-substituted ethylene diminished the problems associated with ^{13}C–^{13}C couplings, which in turn are temperature-dependent because the metallacyclopentane–ethylene complex is fluxional on the NMR timescale.

The aim of these experiments was to determine whether or not the metallacycle was formed exclusively from the coupling of the two coordinated ethylene ligands in **1**, as shown in eq 8. Com-

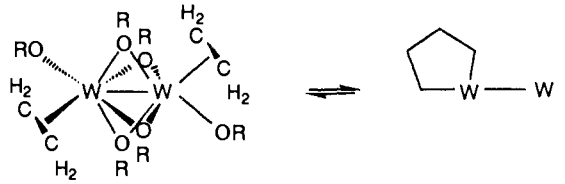

peting with C–C coupling is the reversible formation of **1** from $W_2(OCH_2\text{-}t\text{-}Bu)_6$ and ethylene. The latter reaction scrambles coordinated ethylene with free ethylene. At −32 °C in toluene-d_8, the metallacycle–ethylene complex formation is extremely slow, ca. several months for $t_{1/2}$ for loss of **1**, and we observed scrambling of free and coordinated ethylene after 2 weeks. These labeling experiments are thus inconclusive concerning the coupling of the C_2 units.

We followed the disappearance of **1** in NMR tube reactions in the presence of an excess of ethylene at 22 °C, in toluene-d_8. The added ethylene was estimated to be ca. 10, 20, and 30 equiv, by integration of the ^1H signals of the free and coordinated C_2H_4. The rate of disappearance of the bis-ethylene complex **1** was independent of the free C_2H_4 under these conditions. This rules out a direct attack of a coordinated ethylene ligand of **1** by an entering C_2H_4 molecule. The result is consistent with a rate-determining intramolecular C–C coupling reaction followed by rapid uptake of ethylene.

This proposed reaction pathway complements the observations involving the reactivity of the metallacyclopentane–ethylene complex $W_2(O\text{-}i\text{-}Pr)_6(CH_2)_4(\eta^2\text{-}C_2H_4)$ in the presence of excess $^{13}C_2H_4$. Here, exchange of the η^2-C_2H_4 ligand with added $^{13}C_2H_4$ was much faster than $^{13}C_2H_4$ incorporation into the ring.[7] Given that $W_2(O\text{-}i\text{-}Pr)_6(CH_2)_4(\eta^2\text{-}C_2H_4)$ exists in equilibrium with $W_2(O\text{-}i\text{-}Pr)_6$ and ethylene (3 equiv), this requires that ethylene dissociation precedes decomposition of the metallacyclopentane ring. By microscopic reversibility, the metallacyclopentane ligand must be formed prior to uptake of the kinetically labile η^2-C_2H_4 ligand.

In previous studies of $W_2(CH_2Ph)_2(O\text{-}i\text{-}Pr)_4(\eta^2\text{-}C_2Me_2)_2$ and related bis-alkyne complexes, which are not labile to alkyne dissociation but do show irreversible metallacyclopentadiene formation, the chemistry was straightforward. The rate of coupling of the alkynes was independent of added alkyne, and only the coordinated C_2 units were coupled, eq 9.[35]

$$W_2(CH_2Ph)_2(O\text{-}i\text{-}Pr)_4(\eta^2\text{-}C_2Me_2)_2 + \text{excess } C_2Et_2 \rightarrow HW_2(\mu\text{-}CPh)(\mu\text{-}C_4Me_4)(O\text{-}i\text{-}Pr)_4 + PhCH_3 \quad (9a)$$

$$W_2(CH_2Ph)_2(O\text{-}i\text{-}Pr)_4(\eta^2\text{-}C_2Et_2)_2 + \text{excess } C_2Me_2 \rightarrow HW_2(\mu\text{-}CPh)(\mu\text{-}C_4Et_4)(O\text{-}i\text{-}Pr)_4 + PhCH_3 \quad (9b)$$

Lastly, one may wonder why $W_2(OCH_2\text{-}t\text{-}Bu)_6$ reacts with ethylene to give the bis-ethylene compound **1** as a kinetically persistent intermediate in the formation of the metallacycle–ethylene complex, whereas $W_2(O\text{-}i\text{-}Pr)_6$ and ethylene react rapidly to give $W_2(O\text{-}i\text{-}Pr)_6(CH_2)_4(\eta^2\text{-}C_2H_4)$ without any detectable analogue of **1**. We believe that steric factors are most likely responsible for this subtle difference. If the isopropoxide ligands exert a greater steric pressure at the tungsten centers, the quadruply bridged structure akin to **1** will be destabilized. Alternatively, we could say that the ground-state structure of **1** is stabilized with respect to the activated species required for C–C coupling. Thus, we believe that a doubly bridged intermediate, such as those we described earlier on the basis of edge-shared square-based bipyramids, is most likely involved in metallacycle formation. Perhaps by further studies with different alkoxides, further insight on these matters may be obtained.

It is worth noting that the kinetic lability of the mono-ethylene adduct of $W_2(OCH_2\text{-}t\text{-}Bu)_6$ probably arises from the competitive nature of M–M d_π–d_π and M d_π–C_2 π^* bonding. Coordination of ethylene at one tungsten center will lead to a rehybridization at the metal to allow for W d_π–C_2 π^* bonding, and this in turn will disrupt the W–W π bonding. This will effectively facilitate uptake of the second ethylene ligand. Conversely, elimination of one ethylene from **1** prepares one tungsten atom for incipient W–W triple bond formation upon elimination of the ethylene at the other metal center. Schematically this is shown in eqs 10a and 10b.

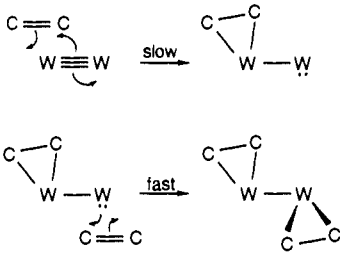

10a

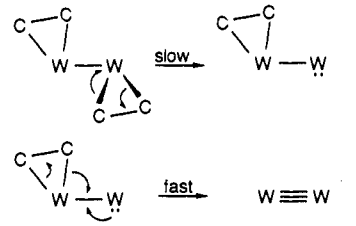

10b

In contrast to our work, Norton and co-workers[36] have studied the reversible addition of ethylene to $Os_2(CO)_8$ which generates a 1,2-dimetallacyclobutane, formally a 2+2 cycloaddition as depicted by eq 11. By analogy, a μ-parallel ethylene adduct of $W_2(OCH_2\text{-}t\text{-}Bu)_6$ would be a 1,2-dimetallacyclobut-1-ene.

$$(CO)_4Os{=}Os(CO)_4 + CH_2{=}CH_2 \rightleftharpoons (CO)_4Os(CH_2{-}CH_2)Os(CO)_4 \quad (11)$$

Concluding Remarks

There are several interesting aspects to this work that reports the first organometallic compound derived from the addition of an olefin, a C–C double bond, to a compound containing a metal–metal triple bond. In particular, we mention the following. (1) The formation of compound **1** is readily reversible at room temperature. Aside from the usual tradeoff between enthalpy and entropy in an equilibrium such as that of eq 4, the key feature here is that metal–olefin and metal–metal bondings are enthapically balanced in the adduct and starting material. (2) The observed structure of **1**, which contains four bridging OR ligands, is unprecedented in the chemistry of adducts of $W_2(OR)_6$ compounds and may be contrasted with the structures seen in the adducts involving allene,[5] crotonaldehyde,[32b] and 1,3-butadiene[6] shown in F, G, and H, respectively. This testifies to the versatility of $W_2(OR)_6$ compounds as templates for substrate uptake and activation.

(35) Chisholm, M. H.; Eichhorn, B. W.; Huffman, J. C. *Organometallics* **1989**, *8*, 67.

(36) (a) Hembre, R. J.; Scott, C. P.; Norton, J. R. *J. Am. Chem. Soc.* **1987**, *109*, 3468. (b) Anson, C. E.; Johnson, B. F. G.; Lewis, J.; Powell, D. B.; Sheppard, N.; Bhattacharya, A. K.; Bender, B. R.; Bullock, R. M.; Hembre, R. T.; Norton, J. R. *J. Chem. Soc., Chem. Commun.* **1989**, 703. (c) Bender, B. R.; Bertoncello, R.; Burke, M. R.; Casarin, M.; Granozzi, G.; Norton, J. R.; Takats, J. *Organometallics* **1989**, *8*, 1777.

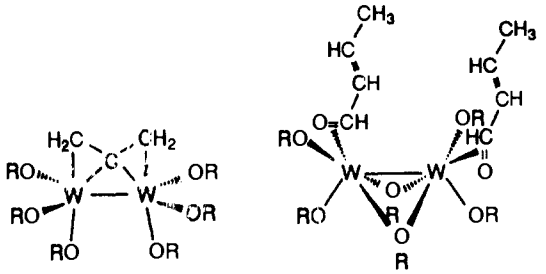

F

G

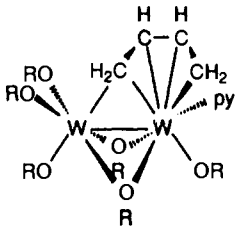

H

Experimental Section

General. NMR samples were prepared from dry and deoxygenated solvents toluene-d_8 and dichloromethane-d_2 in sealed tubes at −72 °C in dry ice/ethanol cooling baths. NMR spectra were run using a Varian XL-300 for ^{1}H NOE and SST studies, and a Bruker AM 500 spectrometer was used for $^{13}C\{^1H\}$ NMR studies.

The temperatures were calculated using Van Geet's equation based on peak separation using the program Temcal(M).[37]

Mass spectra were obtained by Chung-Ping Yu by the method of direct insertion using electron ionization and a Kratos MS80RSAQQ mass spectrometer.

Preparation of $W_2(OCH_2$-t-$Bu)_6(\eta^2$-$C_2H_4)_2$ (1). This was prepared as reported previously[7] with some modifications. A salt–ice bath was substituted for the ice bath to give somewhat lower reaction temperatures (−10 °C). Pentane was used exclusively as solvent since toluene was tedious to remove at low temperature. The ethylene atmosphere was found to be unnecessary during crystal filtration and a nitrogen atmosphere was used. The solution was also able to be reduced in vacuo at −10 °C, and a nearly quantitative yield could be obtained by removal of the solvent in vacuo.

Preparation of $W_2(OCHD$-t-$Bu)_6(C_2H_4)_2$. This was prepared as above using HOCHD-t-Bu rather than neopentyl alcohol. Pivaldehyde was reduced to HOCHD-t-Bu by reaction with $LiAlD_4$.

Nuclear Overhauser Enhancement Studies. NOE experiments were initially run on a sample of $W_2(OCH_2$-t-$Bu)_6(\eta^2$-$C_2H_4)_2$, and then W_2-$(OCHD$-t-$Bu)_6(\eta^2$-$C_2H_4)_2$ was used so that the effects of SST would not obscure the NOE.

In the NMR experiment, D_1, the delay between acquisitions, was set at $4T_1$, and the decoupler power was set as low as possible to give a fully decoupled peak. The interleave function was used with the decoupler set at the frequency of interest and then far off-resonance, 10 000 Hz; 32 scans at each site were generally used, and both spectra and their differences were observed.

Initial single resonance decoupling experiments run at −20 °C established the geminal pairs of the methylenic protons of the neopentoxide ligands to be due to adjacent peaks. The peaks labeled H(1) and H(2) were due to geminal pairs, H(3) and H(4) were geminal pairs, and H(5) and H(6) were geminal pairs in Figure 3.

Nuclear Overhauser enhancement, 10–30%, was always observed between geminal pairs. The NOE results for the ethylenic ligands were consistent with the earlier assignment of the peaks.[7]

The NOE results between ethylenic protons were not quantitative because these peaks were too close in frequency for them to be individually fully decoupled.

The experiments that were used to assign the methylenic protons of the alkoxide ligands involved $W_2(OCHD$-t-$Bu)_6(\eta^2$-$C_2H_4)_2$. NOE was observed between alkoxide methylenic protons and ethylenic protons at −20 °C in CD_2Cl_2. The results are shown in Table VI. The distance between the protons was from the crystal structure data. Protons greater than 2.6 Å apart did not show any NOE.

Spin Saturation Transfer Studies. Spin saturation transfer was observed for $W_2(OCH_2$-t-$Bu)_6(\eta^2$-$C_2H_4)_2$ in toluene-d_8 solution at six temperatures between 5 and 25 °C. A wider temperature range was not possible due to the slow rate of the process at lower temperatures and the fast rate of dissociation of ethylene at higher temperatures. Irradiation was carried out at H(1), and spin saturation transfer was observed at H(4). The exchange between H(5) and H(6) was later checked using $W_2(OCHD$-t-$Bu)_6(\eta^2$-$C_2H_4)_2$ and found to occur at the same rate. At low temperatures H(1) was able to be fully irradiated without the adjacent peak H(2) being affected. The magnitude of the SST was measured from integration of difference spectra. It was assumed that all methylenic alkoxide resonances would have the same integrals. Integration was a large source of error in the experiment. Different runs showed this error to be as large as 20%.

The rates were determined using the equation below, in which M is the magnetization at the site of interest at times 0 and infinity, and T_1 is the relaxation time of the nucleus.[20]

$$k = \frac{M_0 - M_\infty}{M_\infty T_1}$$

T_1 values were measured by using the inversion–recovery technique and the Varian program DOT1.[37] The error in the T_1 values was obtained from the change in T_1 values for the two peaks from the doublet.

These data are found in Table VII. The error in the final values was determined from a least-squares analysis of six points.

The correlation coefficient for Eyring and Arrhenius plots was found to be 0.991. The following values were obtained by least-squares analysis: $\log A = 10.4 \pm 0.7$, $E_{act} = 14 \pm 1$ kcal mol^{-1}, $\Delta H^* = 14 \pm 1$ kcal mol^{-1}, $\Delta S^* = -13 \pm 3$ cal K^{-1} mol^{-1}.

Kinetic Studies. Measurement of Decrease in $[W_2(OCH_2$-t-$Bu)_6(\eta^2$-$C_2H_4)_2]$ with Time with Different Amounts of Added C_2H_4. W_2-$(OCH_2$-t-$Bu)_6$ (~50 mg, ~0.06 mmol) was placed in a 25-mL Schlenk flask, and 2.5 mL of toluene-d_8 was added at −72 °C (dry ice/ethanol) due to the thermal instability of $W_2(OCH_2$-t-$Bu)_6$ which dimerizes to form $W_4(OCH_2$-t-$Bu)_{12}$ at room temperature. The solid was well-dissolved, and 0.4 mL of the solution was transferred to each of three NMR tubes at −72 °C under N_2(g) atmosphere. The solutions were frozen, and 0.23, 0.15, and 0.076 mmol $^{13}C^{12}CH_4$ were added to the three tubes, respectively, using a calibrated vacuum manifold. The tubes were sealed with a torch.

Each in turn, the tubes were warmed to room temperature. Initial ^{1}H NMR spectra were run, which showed only the presence of free $^{13}CCH_4$ and $W_2(OCH_2$-t-$Bu)_6(\eta^2$-$^{13}CCH_4)_2$, and used to determine the amount of free ethylene to $W_2(OCH_2$-t-$Bu)_6$, which was 30, 20, and 10 equiv, respectively. The decrease in $W_2(OCH_2$-t-$Bu)_6(\eta^2$-$^{13}CCH_4)_2$ was then monitored by $^{13}C\{^1H\}$ NMR spectroscopy at 125.76 MHz with respect to the toluene-d_8 methyl signal at δ 20.4 as integral 1. The results are listed in Table VIII.

Table VIII. Decrease in $[W_2(OCH_2$-t-$Bu)_6(^{13}CCH_4)_2]$ with Time in the Presence of Added $^{13}CCH_4$

10 equiv $^{13}CCH_4$		20 equiv $^{13}CCH_4$		30 equiv $^{13}CCH_4$	
time (min)	integral[a]	time (min)	integral	time (min)	integral
		4	1.91	5	1.76
29	1.47	9	1.89	14	1.84
38	1.28	16	1.82	33	1.45
47	1.22	25	1.63	57	1.26
56	1.18	34	1.51	73	1.11
70	1.14	45	1.38	86	1.03
141	0.90	68	1.33	104	0.89
159	0.97	97	1.22	132	0.82
219	0.81	153	1.08	155	0.73

[a] Integrals were measured relative to the toluene-d_8 methyl signal at δ 20.4 as **1**.

Crystallographic Studies. General operating procedures and listings of programs have been described previously.[38]

A suitable crystal was selected and transferred to the goniostat where it was cooled to −155 °C for characterization and data collection. A systematic search of a limited hemisphere of reciprocal space located a set of diffraction maxima with symmetry and systematic absences corresponding to the unique monoclinic space group $P2_1/c$. Subsequent solution and refinement of the structure confirmed this choice. The

(37) Patt, S. *XL-Series Basic Operation Manual*; Publication No. 87-146-054; Varian Instrument Division: Palo Alto, 1985; pp 3–16, 7–19.

(38) Chisholm, M. H.; Folting, K.; Huffman, J. C.; Kirkpatrick, C. C. *Inorg. Chem.* **1984**, *23*, 1021.

structure was solved by a combination of direct methods and Fourier techniques. All hydrogen atoms were clearly visible in a difference Fourier synthesis phased on the non-hydrogen parameters. All hydrogen atoms were refined isotropically and non-hydrogen atoms anisotropically in the final cycles.

A final difference Fourier map was featureless, with the two largest peaks of 1.3 e/Å^3 each lying within 0.5 Å of the two W atoms. All other peaks were less than 0.7 e/Å^3.

Computational Procedures. Molecular orbital calculations were performed on a VAX computer system using the semiempirical methods of Fenske–Hall[21] and extended Hückel.[30] For the Fenske–Hall calculations, atomic wave functions were supplied by Professor M. B. Hall from Texas A&M University. Contracted double-ζ representations were used for the W 5d, O 2p, and C 2p atomic orbitals. In the basis function for tungsten, the 6s and 6p exponents were fixed at 2.40. All Fenske–Hall calculations were converted with a self-consistent field iterative technique by using a convergence criteria of 0.0010 as the largest deviation between atomic orbital populations for successive cycles.

The calculations were carried out on the hypothetical molecule $W_2(OH)_6(\eta^2\text{-}C_2H_4)_2$. The OH and CH bond distances were set at 0.96 and 1.08 Å, respectively, and other distances were obtained from the crystal structure or adapted to C_2 symmetry. The W–O terminal distances were set at 1.888 Å and W–O bridging distances in the asymmetric structure were 2.309 and 1.993 Å. Symmetric bridges had W–O distances of 2.15 Å. The W–C bond distance was averaged to 1.45 Å. The hydroxide ligands and the centroid of the ethylene C–C bonds were idealized so as to lie in two mutually perpendicular planes. The C–C bond axis of the ethylene ligand was oriented perpendicular to the plane containing the tungsten atom, the terminal OH ligand, and the C–C midpoint. In the Fenske–Hall calculations, the terminal OH bonds were constrained to be linear and the bridging hydroxide bonds planar, and the OH group was pointing such that it was perpendicular to the W–W bond axis.

The structural parameters for the intermediate in the fluxional process came from a combination of the crystal structure of $W_2(OCH_2\text{-}t\text{-}Bu)_6(\eta^2\text{-}C_2H_4)_2$ and $W_2(CH_2Ph)_2(O\text{-}i\text{-}Pr)_4(\eta^2\text{-}C_2Me_2)_2$.[32a] The distances were taken from $W_2(OCH_2\text{-}t\text{-}Bu)_6(\eta^2\text{-}C_2H_4)_2$, and the angles were taken from $W_2(CH_2Ph)_2(O\text{-}i\text{-}Pr)_4(\eta^2\text{-}C_2Me_2)_2$, in that the geometry about each W atom was taken to be square pyramidal with the alkoxide ligands occupying the base of the pyramid. In the latter molecule the bridges are asymmetric, but here they were made to be symmetric. The molecule was idealized to C_{2v} symmetry. With the structural parameters chosen in this way, the structure has not been optimized.

The extended Hückel calculations that examined the trans influence of the terminal ligands used W–O–C angles of the crystal structure for the W–O–H angles, although the addition of these angles was not found to change the results significantly.

Acknowledgment. We thank the Department of Energy, Office of Energy Research, Division of Chemical Sciences, for support. S.T.C. thanks the American Association of University Women Educational Foundation for an American Dissertation Year Fellowship. The Laboratoire de Chimie Théorique is associated with the CNRS (URA 506) and member of ICMO and IPCM. We also thank the NSF and CNRS under the US–France Cooperative Science Program.

Supplementary Material Available: Tables of anisotropic thermal parameters, complete listings of bond distances and bond angles, VERSORT drawings, and an Arrhenius plot of the kinetic data (13 pages); listing of F_o and F_c values (12 pages). Ordering information is given on any current masthead page.

Magnetic Properties of High-Nuclearity Spin Clusters. Fourteen- and Fifteen-Oxovanadium(IV) Clusters

Anne-Laure Barra,[†,§] Dante Gatteschi,*[,†] Luca Pardi,[†] Achim Müller,*[,‡] and Joachim Döring[‡]

Contribution from the Department of Chemistry, University of Florence, Florence, Italy, and Fakultät für Chemie, Universität Bielefeld, Bielefeld, Germany. *Received March 6, 1992*

Abstract: The magnetic properties of $K_6[V_{15}As_6O_{42}(H_2O)]\cdot 8H_2O$ (V_{15}) and $(NH_4)_6[V_{14}As_8O_{42}(SO_3)]$ (V_{14}) which comprise fifteen- and fourteen-vanadium(IV) ions, respectively, have been investigated. The analysis of the magnetic susceptibility and of the EPR spectra showed the presence of several different exchange pathways, which were identified also with the help of extended Hückel calculations. The analysis of the data was performed using both a perturbation and a rigorous approach within the spin hamiltonian formalism, allowing for the first time a deep insight into the energy levels of high nuclearity spin clusters.

Introduction

Molecular materials are actively investigated because with the approaches of molecular chemistry it is possible to fine tune their properties and obtain materials that can perform many of the functions traditionally associated with two- and three-dimensional network solids.[1-6]

One of the fields where exciting developments are reported almost every month is that of molecular based magnetic materials.[2,7-13] In this area several attempts have been made to design and synthesize "organic ferromagnets" or molecular materials exhibiting spontaneous magnetization below a critical temperature.

Another area of turmoil is that of high nuclearity spin clusters, HNSC, i.e. molecular materials containing large, but finite, numbers of spins which are coupled to each other.[14-18] For instance, manganese clusters containing up to 12 ions[19,20] and iron clusters containing up to 17 ions[21] recently have been reported in connection with the investigation of molecular models of bio-

[†] University of Florence.
[§] On leave of absence from SNCI, CNRS, Grenoble.
[‡] University of Bielefeld.

(1) Miller, J. S. *Adv. Mater* **1990**, *2*, 98.
(2) *Magnetic Molecular Materials*; Gatteschi, D.; Kahn, O.; Miller, J. S.; Palacio, F., Eds.; Kluwer: Dordrecht, 1991.
(3) *Molecular Electronic Devices*; Carter, F. L., Ed.; Marcel Dekker: New York, 1982. *Molecular Electronic Devices II*; Carter, F. L., Ed., Marcel Dekker: New York, 1987.
(4) *Materials for Nonlinear Optics, Chemical Perspectives*; Mardez, S. R.; Sohn, J. E.; Stucky, G. D.; ACS Symposium Series No. 455; American Chemical Society: Washington, DC, 1991.
(5) Kini, A. M.; Geiser, U.; Wang, H. H.; Carlson, K. D.; Williams, J. M.; Kwok, W. K.; Vandervoort, K. G.; Thompson, J. E.; Stupka, D. L.; Jung, D.; Whangbo, M. H. *Inorg. Chem.* **1990**, *29*, 2555.
(6) Manriquez, J. M.; Yee, G. T.; Scott McLean, R.; Epstein, A. J.; Miller, J. S. *Science* **1991**, *252*, 1415.
(7) Broderick, W. E.; Thompson, J. A.; Day, E. P.; Hoffman, M. *Science* **1990**, *249*, 910.
(8) Caneschi, A.; Gatteschi, D.; Rey, P. *Prog. Inorg. Chem.* **1991**, 39.
(9) Allamand, P. M.; Khemani, K. C.; Koch, A.; Wudl, F.; Holczer, K.; Donovan, S.; Gruener, G.; Thompson, J. D. *Science* **1991**, *253*, 301.

0002-7863/92/1514-8509$03.00/0